Stem Cell Reports
Article

OPEN ACCESS

CGG Repeat-Induced *FMR1* Silencing Depends on the Expansion Size in Human iPSCs and Neurons Carrying Unmethylated Full Mutations

Urszula Brykczynska,[1] Eline Pecho-Vrieseling,[1] Anke Thiemeyer,[1] Jessica Klein,[1] Isabelle Fruh,[1] Thierry Doll,[1] Carole Manneville,[1] Sascha Fuchs,[1] Mariavittoria Iazeolla,[1] Martin Beibel,[1] Guglielmo Roma,[1] Ulrike Naumann,[1] Nicholas Kelley,[1] Edward J. Oakeley,[1] Matthias Mueller,[1] Baltazar Gomez-Mancilla,[1] Marc Bühler,[2,3] Elisabetta Tabolacci,[4] Pietro Chiurazzi,[4] Giovanni Neri,[4] Tewis Bouwmeester,[1] Francesco Paolo Di Giorgio,[1,*] and Barna D. Fodor[1,*]

[1]Novartis Institutes for Biomedical Research, 4056 Basel, Switzerland
[2]Friedrich Miescher Institute for Biomedical Research, 4058 Basel, Switzerland
[3]University of Basel, 4003 Basel, Switzerland
[4]Institute of Genomic Medicine, Catholic University, 00168 Rome, Italy
*Correspondence: francesco.di_giorgio@novartis.com (F.P.D.G.), barna.fodor@novartis.com (B.D.F.)
http://dx.doi.org/10.1016/j.stemcr.2016.10.004

SUMMARY

In fragile X syndrome (FXS), CGG repeat expansion greater than 200 triplets is believed to trigger *FMR1* gene silencing and disease etiology. However, FXS siblings have been identified with more than 200 CGGs, termed unmethylated full mutation (UFM) carriers, without gene silencing and disease symptoms. Here, we show that hypomethylation of the *FMR1* promoter is maintained in induced pluripotent stem cells (iPSCs) derived from two UFM individuals. However, a subset of iPSC clones with large CGG expansions carries silenced *FMR1*. Furthermore, we demonstrate de novo silencing upon expansion of the CGG repeat size. *FMR1* does not undergo silencing during neuronal differentiation of UFM iPSCs, and expression of large unmethylated CGG repeats has phenotypic consequences resulting in neurodegenerative features. Our data suggest that UFM individuals do not lack the cell-intrinsic ability to silence *FMR1* and that inter-individual variability in the CGG repeat size required for silencing exists in the FXS population.

INTRODUCTION

FMR1 is an X-linked gene containing an array of CGG repeats located within the 5′ UTR, which normally range from 6 to 55 and may be unstable upon transmission to the next generation (Biancalana et al., 2015).

Repeat numbers from 55 to 200, so-called premutation, result in expression of mRNA with expanded CGG repeats. Individuals carrying the premutation are at risk of developing fragile X tremor ataxia syndrome (FXTAS, OMIM #300623), a late-onset neurodegenerative disease (Hagerman et al., 2001). One of the hallmarks of this disease is ubiquitin-positive inclusion bodies, which have been detected in postmortem brain samples (Greco et al., 2006).

A repeat expansion of more than 200 triplets (full mutation) triggers gene silencing of *FMR1*, causing fragile X syndrome (FXS, OMIM #300624), the most common inherited form of intellectual disability and autism (Verkerk et al., 1991). Silencing is initiated during early embryonic development and involves establishment of heterochromatin at the *FMR1* promoter, including DNA methylation (Sutcliffe et al., 1992). *FMR1* encodes the fragile X mental retardation protein (FMRP) and its absence impairs synaptic functions (Willemsen et al., 2011).

Mosaicism in CGG repeat length is often observed in FXS patients, who carry both premutation and full mutation alleles and therefore differ in the proportion of cells with silenced *FMR1*, which contributes to the clinical spectrum of FXS phenotypes (Rousseau et al., 1994). Mosaicism in the methylation pattern of the expanded CGG repeats has also been described (Hagerman et al., 1994). So-called unmethylated full mutation (UFM) individuals represent an extreme case with all expanded alleles above 200 CGG repeats being unmethylated. These individuals display no signs of intellectual disability (Smeets et al., 1995; Tabolacci et al., 2008; Wohrle et al., 1998) and only a handful of cases have been identified worldwide. Molecular properties of the *FMR1* promoter have been studied in lymphoblastoid cell lines and primary fibroblasts derived from UFM individuals (Pietrobono et al., 2005; Tabolacci et al., 2008). Normal or slightly elevated *FMR1* transcription, with reduced FMRP level due to translational inefficiency, as well as euchromatic configuration of the *FMR1* promoter have been demonstrated in these lines (Pietrobono et al., 2005; Tabolacci et al., 2008). However, it is not clear whether these cells have completely lost the ability to methylate *FMR1*.

Human embryonic stem cells (ESCs) with more than 200 CGG repeats in the *FMR1* locus as well as induced pluripotent stem cells (iPSCs) from FXS patients have been used to study the disease properties at a cellular level (Avitzour et al., 2014; Colak et al., 2014; Eiges et al., 2007; Sheridan et al., 2011; Telias et al., 2013; Urbach et al., 2010). These human ESCs serve as a model for developmental silencing of *FMR1*. In a fraction of ESC lines *FMR1* is already repressed, whereas in some it is still active and

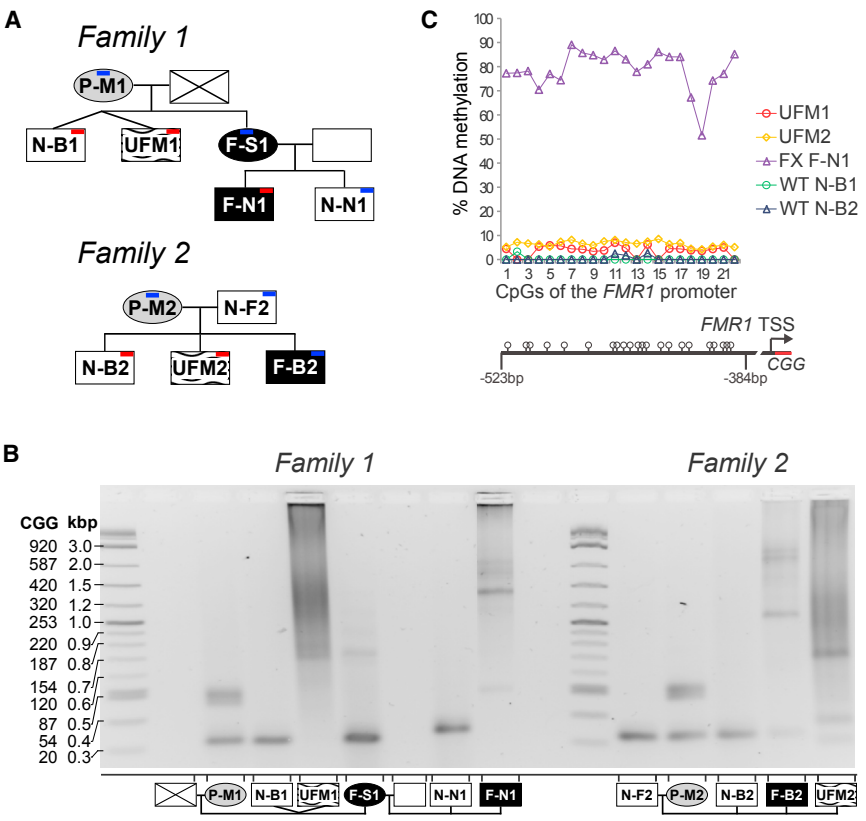

Figure 1. UFM Families

(A) Pedigrees of families with UFM subjects. Oval, female; square, male; crossed, deceased; white, normal; gray, premutation; black, FXS; black on white pattern, UFM; blue, buccal swap sample; red, blood sample.

(B) CGG repeat size in 5′ UTR of *FMR1* analyzed by PCR in UFMs and their families' members. Additional analysis of the expansion size by capillary electrophoresis in UFM2 is provided in Figure S1.

(C) Percentage DNA methylation of 22 CpGs of the *FMR1* promoter analyzed by bisulfite pyrosequencing in PBMC population. UFM individuals display a minor proportion of methylated alleles. Graph based on data in Table S1.

becomes silenced during in vitro neuronal differentiation (Avitzour et al., 2014; Colak et al., 2014). In contrast, iPSCs derived from FXS patients do not reactivate *FMR1*, suggesting that the gene is locked in a silenced state that is resistant to epigenetic reprogramming (Sheridan et al., 2011; Urbach et al., 2010). Therefore, these cells are not used to study the mechanism of *FMR1* silencing, but for modeling of neurological phenotypes of FXS (Sheridan et al., 2011; Telias et al., 2013). In a recent study, iPSCs have been also derived from one UFM individual (de Esch et al., 2014). It has been reported that the cells gained silencing of the *FMR1* promoter upon reprogramming, hindering the use of these cells for further analyses of the UFM phenotype.

In this study we used somatic reprogramming to dissect the relationship between repeat lengths and silencing status in iPSCs from two unrelated UFM individuals. We found that in the majority of iPSC clones *FMR1* remained unmethylated and active. However, in a small proportion of clones which carried more than 400 CGGs *FMR1* was silenced, suggesting that the CGG repeat number necessary to induce the silencing is ~400 in UFM individuals and not ~200 as described for FXS. Moreover, we demonstrate that upon selective pressure, unmethylated UFM clones gained methylation accompanied by an expansion of the CGG repeats above this higher threshold.

Furthermore, the persistence of the UFM phenotype in iPSC-derived neurons allowed us to investigate whether cells carrying the expanded CGG repeat number and active *FMR1* develop a neurodegenerative phenotype. Indeed, we found ubiquitin inclusion bodies in these cells, a phenotypic feature of FXTAS patients. We also observed that in UFM as well as in premutation, iPSC-derived neurons form FMRP inclusions that may contribute to the FXTAS pathology.

RESULTS

Genetic and Epigenetic Characterization of *FMR1* Locus in UFM Individuals

Here we describe one previously reported (Pietrobono et al., 2005; Tabolacci et al., 2008) and one new UFM individual, identified within two unrelated FXS families (Figure 1A). Blood samples were obtained from both UFM individuals, from their two healthy brothers N-B1 and N-B2, and the FXS nephew of UFM1, F-N1 (Figure 1A). In addition, we sampled buccal swabs from the additional living members of the families (Figure 1A). For all, we determined CGG repeat length by PCR amplification (Figure 1B). The full expansion status (greater than 200 CGGs) was confirmed for UFM and FXS individuals, as well as the premutation

status of their mothers. As expected, in premutation and full mutation females we detected both expanded and wild-type (WT) alleles. The CGG repeat expansion of UFM individuals did not have a discrete length but displayed a continuous spectrum of sizes. This pattern is observed for all reported UFM individuals to date and is attributed to the somatic instability of unmethylated repeats (Biancalana et al., 2015). For UFM1 repeat sizes ranged from 200 to 500 CGGs and for UFM2 premutation bands of 50 and 150 and a smear from 200 to 370 repeats were detected, indicating a mosaic status between a premutation and full mutation (Figure 1B). Southern blot analysis and capillary electrophoresis gave comparable results for UFM1 (Tabolacci et al., 2008) and UFM2, respectively (Figure S1).

We compared the DNA methylation status of the *FMR1* promoter in the most closely related male individuals with UFM, WT, and FXS phenotypes. We analyzed 22 CpGs within the *FMR1* promoter using bisulfite pyrosequencing in peripheral blood mononuclear cells (PBMCs) purified from blood. In cells from both UFMs the mean DNA methylation was 4% and 6% for UFM1 and UFM2, respectively, compared with 0.1% and 0.3% in two WT (N-B1 and N-B2) individuals and 79% in an FXS patient (F-N1) (Figure 1C and Table S1). The low level of methylation in UFM PBMCs suggests the presence of fully methylated alleles and, therefore, a low level of methylation mosaicism in these individuals.

CGG Repeat Sizes and *FMR1* Expression States in UFM iPSC Clones

PBMCs are composed of cells with heterogeneous CGG repeat size and the *FMR1* promoter methylation status. To dissect the relationship between repeat size, methylation status, and *FMR1* expression, we derived iPSCs from PBMCs and performed analyses on multiple distinct clones.

Activated T cells were used for somatic reprogramming by Sendai viruses harboring the SOX2, OCT4, c-MYC, and KLF4 reprogramming factors (Takahashi et al., 2007). A total of 11–12 clones were characterized from each individual. All clones expressed markers of pluripotency (Figure S2A) and were analyzed for the CGG repeat size, the DNA methylation status of the promoter, and the expression level of *FMR1* (Figure 2 and Table S1).

The majority of clones obtained from both UFM individuals had repeat sizes corresponding to the spectrum of sizes observed in the PBMCs (Figure 2A). Three clones from UFM1 displayed shorter CGG repeat sizes, with either WT (UFM1-1) or premutation (UFM1-2 and UFM1-3) size. This may represent either a contraction event or preexisting lowly abundant alleles in the original PBMC samples.

The majority of UFM clones with repeat sizes above 200 CGGs retained the hypomethylated *FMR1* promoter and expressed *FMR1* at levels comparable with WT (Figure 2). Most of them showed discrete repeat sizes as expected from the iPSC clonal derivation procedure. All clones were analyzed between passages 5 and 10. A representative UFM clone UFM1-5 was followed until passage 22 and showed no changes in the hypomethylated status of the *FMR1* promoter and only slight CGG repeat instability (Figure S2B). We conclude that the UFM phenotype is stable upon somatic reprogramming and is maintained in iPSCs.

Interestingly, 2 of 11 clones from UFM1 (UFM1-10 and UFM1-11) with the highest CGG repeat sizes (>450 CGGs) were hypermethylated and did not express *FMR1*. In UFM2 we also identified 1 of 12 clones (UFM2-12) that was silenced, hypermethylated, and carried more than 400 CGGs. However, a second silenced clone from UFM2 (UFM2-4) carried less than 200 CGGs. These silenced clones may originate from the 5% methylated alleles in PBMC samples or represent a de novo silencing event during reprogramming.

We conclude that in the UFM individuals analyzed in this study, the silencing threshold lies at 450 repeats in UFM1 and 400 repeats in UFM2 (yellow lines in Figure 2A). However, this threshold is less evident in UFM2 where an outlier clone, UFM2-4, has been identified.

Silencing Threshold of CGG Repeat Length in FXS iPSCs

The above results prompted us to investigate whether the increased silencing threshold is a property exclusive to these two UFM individuals. To this end, we analyzed iPSCs from FXS patient F-N1, a nephew of UFM1 (Figure 3). In the majority of F-N1 clones the *FMR1* promoter was fully methylated, an observation in line with the described resistance of *FMR1* silencing to the somatic reprogramming (Sheridan et al., 2011; Urbach et al., 2010). However, we also identified two clones with active *FMR1* (F-N1-1 and F-N1-2) and repeat sizes above 200 CGG, but shorter than in the silenced clones. The majority of the alleles in these clones were hypomethylated (Figure 3 and Table S1). We conclude that in this FXS patient the silencing threshold lies around 400 CGG (yellow line in Figure 3A). Clones carrying the same size of 420 CGG were active in UFM1 (UFM1-7, UFM1-8, UFM1-9) and silenced in F-N1 (FN1-3).

We also derived iPSCs from an FXS individual not related to the UFM families, from which iPSCs with the active unmethylated full mutation allele of *FMR1* have been previously described (Avitzour et al., 2014). Similarly to the previous report, one of three analyzed clones was active and fully unmethylated (Figure 3). The repeat size of this clone ranged from 250 to 320 CGGs. A faint premutation band of 80 CGGs was also detected. Nevertheless, 98% of alleles were unmethylated. A smear indicating instability of active expanded alleles was also observed. Consistent

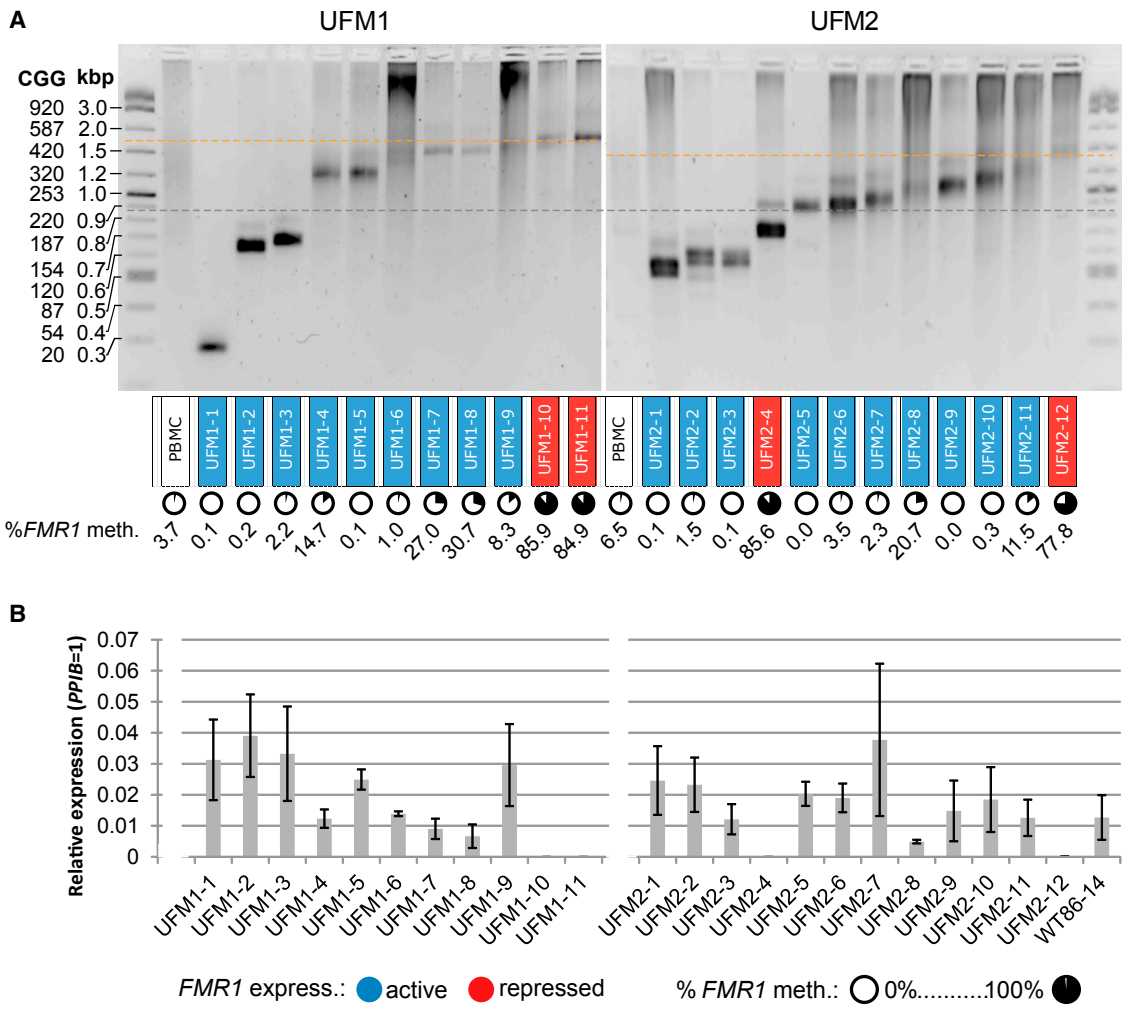

Figure 2. Increased Silencing Threshold in iPSC Clones Derived from UFM Subjects

(A) CGG repeat size in 5′ UTR of *FMR1* analyzed by PCR in iPSCs derived from PBMCs from UFM1 and UFM2. Background color of a clone name indicates expression of *FMR1* based on data in (B), expressing (blue), not expressing, or expressing below 5% of WT level (red). Circles under the clone names indicate mean percentage of DNA methylation across 22 CpGs of the *FMR1* promoter based on data in Table S1. Silent and fully methylated clones are observed in both UFM subjects. Yellow lines indicate the proposed approximate thresholds of CGG repeat numbers triggering *FMR1* silencing in a given individual. The grey line corresponds to 200 CGG repeats. See also Figure S2.

(B) Expression of *FMR1* mRNA in iPSC clones from PBMCs from UFM1 and UFM2 analyzed by TaqMan assay. WT iPSC clone 86-14 derived from a normal individual is included as a WT reference. Data are presented as a mean of three independent biological replicates. Error bars represent SD.

with a shift of the repeat threshold in this individual, the two silenced clones FX97-2 and FX97-3 had repeat sizes larger than 400 CGGs. We conclude that the threshold in CGG repeat size resulting in silencing of *FMR1* is subject to inter-individual variation not only in UFM individuals but also in a proportion of FXS patients.

De Novo Methylation of *FMR1* in UFM iPSCs Is Coupled with an Increase in the CGG Repeat Size

To assess whether UFM cells have intrinsic capacity to de novo silence the *FMR1* locus, we evaluated whether an active allele with a given repeat size can spontaneously gain DNA methylation. Under extended cell culture up to passage 22 we did not observe a spontaneous appearance of methylated alleles for a representative clone UFM1-5 (Figure S2B). Therefore, we established a genetic system to select for *FMR1* silencing events. Our approach was based on the fact that replicating mammalian cells expressing the herpes simplex virus thymidine kinase (HSV-TK) enzyme become sensitive to the prodrug ganciclovir causing cell lethality, while non-expressing cells survive and proliferate upon treatment. We deployed genome

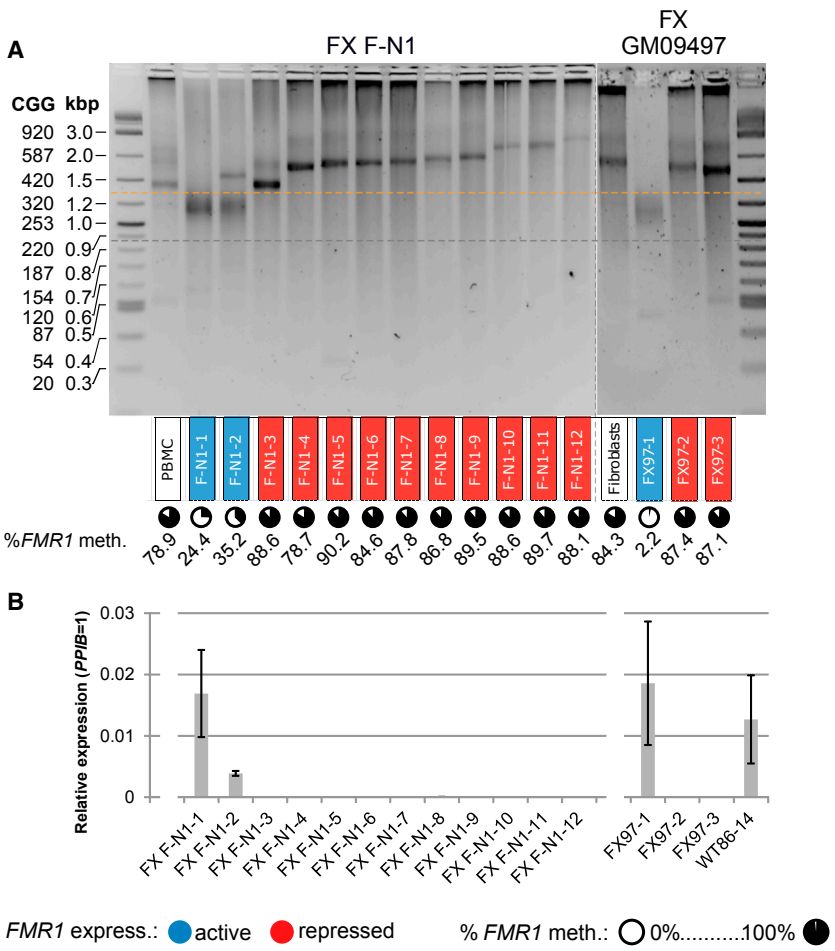

Figure 3. UFM-Like Clones and Altered Silencing Threshold in iPSCs Derived from FXS Patients

(A) CGG repeat size in 5′ UTR of *FMR1* analyzed by PCR in iPSC clones derived from FXS patients. Background color of a clone name indicates expression of *FMR1* based on data in (B), expressing (blue), not expressing or expressing below 5% of WT level (red). Circles under the clone names indicate mean percentage of DNA methylation across 22 CpGs of the *FMR1* promoter based on data in Table S1. Active, hypomethylated clones with more than 200 CGGs are observed in both FXS patients. Yellow line indicates the proposed approximate threshold of CGG repeat numbers triggering *FMR1* silencing in these individuals. The grey line corresponds to 200 CGG repeats.

(B) Expression of *FMR1* mRNA in iPSC clones derived from FXS patients analyzed by TaqMan assay. WT iPSC clone 86-14 derived from a normal individual is included as a WT reference. Data are presented as a mean of three independent biological replicates. Error bars represent SD.

engineering to drive expression of a hygromycin-HSV-TK fusion protein from the endogenous *FMR1* promoter (Figure 4A).

We inserted a selection cassette coding for a fusion of a P2a peptide-hygromycin-HSV-thymidine kinase (Hyg-TK) protein into exon 4 of the *FMR1* gene in iPSC clone UFM1-5 using the CRISPR/Cas9 system (Figures 4A and S3A). This setup allowed for the direct hygromycin selection of correct insertions. After selection of clones we confirmed a single integration event and analyzed their CGG repeat length, *FMR1* methylation, and mRNA expression (Figures S3B–S3E). The clones were maintained in hygromycin-supplemented medium to assure the absence of cells with methylated *FMR1* promoter. Two clones, UFM1-5-6 and UFM1-5-7, with 250 and 320 CGG repeats, respectively, were selected for further experiments. Unlike the parental line UFM1-5 (Figure S3F), the knockin clones were ganciclovir sensitive at concentrations of 5 and 10 μM after 3 days of prodrug treatment in the absence of hygromycin (Figures 4B, 4C, and S3F). To allow the appearance of spontaneous *FMR1* silencing events, we cultured cells without hygromycin for 4 weeks (~8 passages). Subsequent selection for silenced clones was performed using 10 μM ganciclovir for 3 days. The 4 weeks of hygromycin withdrawal was necessary to observe reproducible appearance of ganciclovir-resistant clones in UFM1-5-7, and ganciclovir selection after shorter periods of hygromycin withdrawal yielded no survivals. For the line UFM1-5-6 we did not observe any stable ganciclovir-resistant clones (Figure 4D).

Most ganciclovir selected subclones did not survive passaging, especially the ones which lost the iPSC morphology. Importantly, we identified two clones with iPSC morphology and stable ganciclovir resistance (Figure 4E). Both subclones UFM1-5-7-1 and UFM1-5-7-2 showed full methylation of the *FMR1* promoter and CGG repeat sizes of ~800 CGGs, indicating that the expansion of the CGG repeat led to the silencing of *FMR1*. We used clone UFM1-5-7-1 in a follow-up experiment to test the reversibility of the CGG expansion and methylation by applying hygromycin selection. Interestingly, upon withdrawal of ganciclovir we observed the appearance of

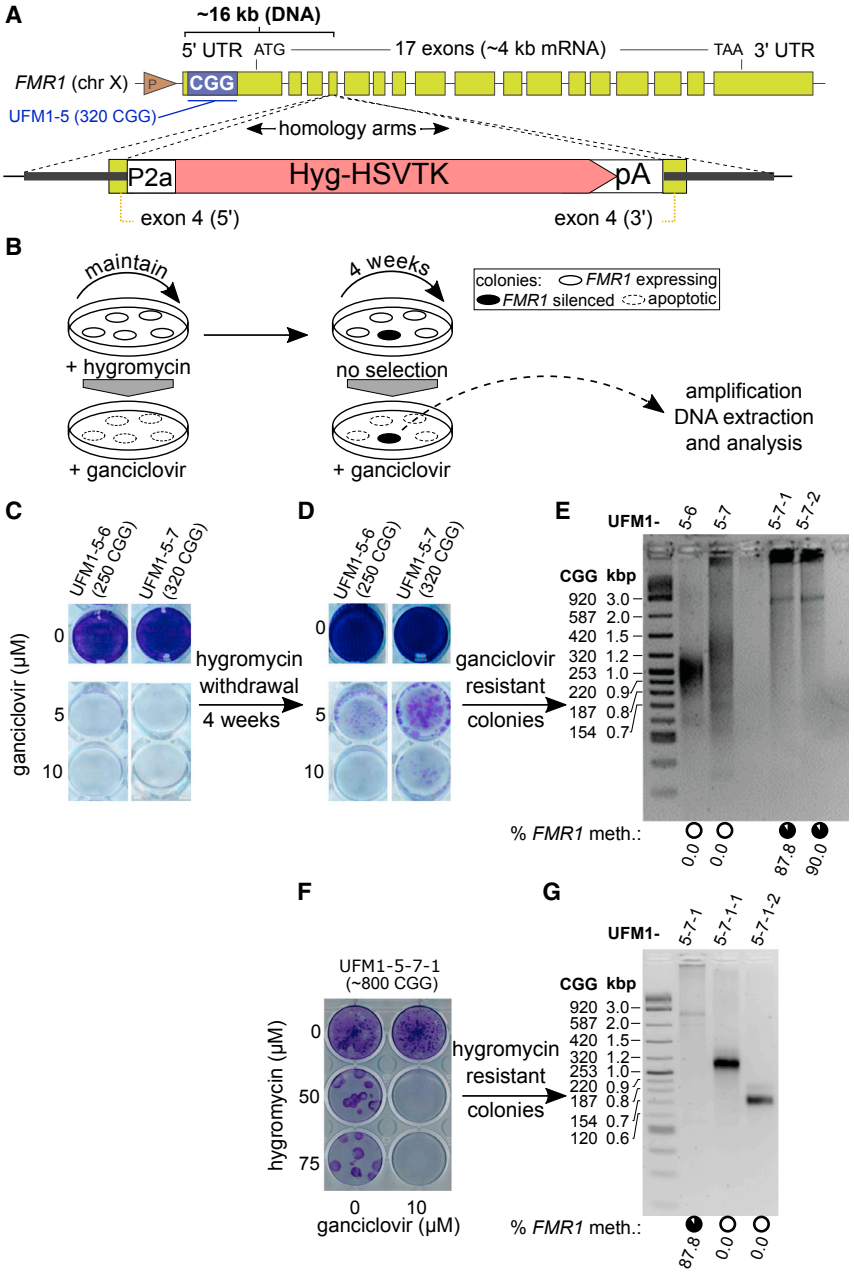

Figure 4. Gain in CGG Repeat Number Is Coupled with *FMR1* Silencing in UFM iPSC Clones

(A) Strategy to target a hygromycin resistance-HSV thymidine kinase (HyTK) positive/negative selection cassette into *FMR1*. In this setup transgene expression is driven by the endogenous *FMR1* promoter. See also Figure S3.

(B) Experimental design to select for iPSCs that silence the *FMR1* promoter driven HyTK. Continuous hygromycin administration selects for cells that express the transgene making them sensitive to ganciclovir. Four weeks without hygromycin allows appearance of cells that spontaneously downregulate the transgene. These cells can be selected for by ganciclovir treatment. Subsequent DNA analysis identifies clones with *FMR1* promoter methylation events.

(C and D) Crystal violet staining of surviving cells after ganciclovir treatment of two knockin iPSC clones (UFM1-5-6 and UFM1-5-7) that were maintained: (C) under hygromycin selection or (D) without hygromycin selection for 4 weeks.

(E) DNA methylation status and number of CGG repeats of *FMR1* from knockin iPSC lines before and after hygromycin withdrawal and subsequent ganciclovir selection. Lanes UFM1-5-6 and UFM1-5-7 are the original clones before hygromycin withdrawal. Subclones UFM1-5-7-1 and UFM1-5-7-2 are derived from UFM1-5-7 after 4 weeks of hygromycin withdrawal and subsequent ganciclovir selection. Circles under each lane indicate mean percentage of DNA methylation across 22 CpGs of the *FMR1* promoter for a given line based on data in Table S1. Two ganciclovir-resistant clones, UFM1-5-7-1 and UFM1-5-7-2, gained ~90% methylation and have increased CGG repeats (~800 CGG) compared with the parental UFM1-5-7 (320 CGG). See also Figure S4.

(F) Crystal violet staining of surviving cells after hygromycin treatment of ganciclovir-resistant subclone UFM1-5-7-1. For cells maintained with ganciclovir, no surviving colonies are observed. Upon ganciclovir withdrawal, spontaneous reactivation of *FMR1* promoter is possible and appearance of surviving colonies is observed.

(G) Analysis of two hygromycin-resistant colonies obtained from subclone UFM1-5-7-1 after withdrawal of ganciclovir as indicated in (F). Parental clone UFM1-5-7 is analyzed in the first lane for direct comparison. CGG repeat sizes 320 and 150 indicate contraction events. Black circles under each lane indicate mean percentage of DNA methylation across 22 CpGs of the *FMR1* promoter based on data in Table S1. No methylation is observed in the surviving colonies, indicating that contraction below the silencing threshold is associated with loss of DNA methylation.

"revertant" hygromycin-resistant clones which coincided with contraction of CGG repeats and loss of DNA methylation (Figures 4F and 4G).

We conclude that the silencing of *FMR1* in UFM iPSCs directly depends on the size of the CGG repeat. Furthermore, UFM cells have not lost the capacity to silence

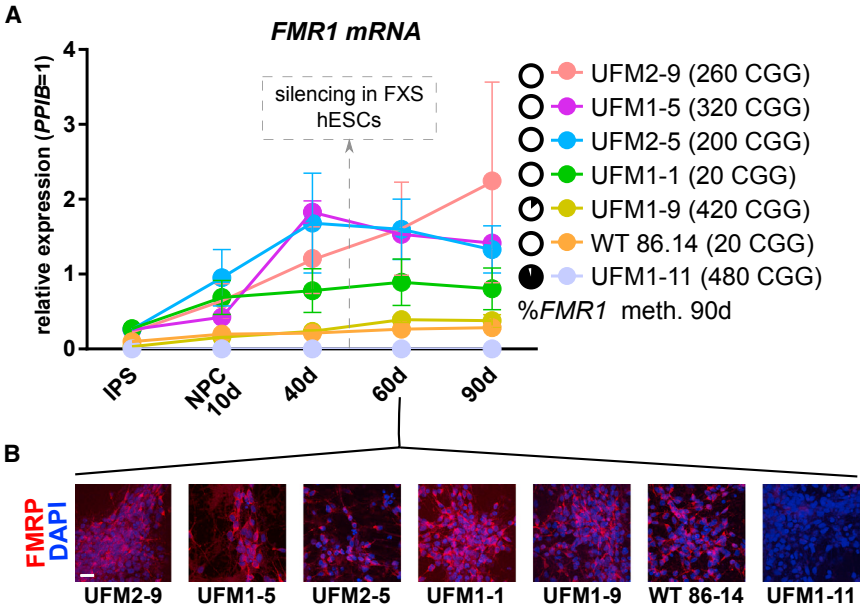

Figure 5. UFM iPSC Derived Neurons Do Not Undergo Developmental Silencing of *FMR1*

(A) Expression of *FMR1* mRNA during 90 days of neuronal differentiation of iPSC lines with variable repeat length and methylation. Timing of *FMR1* silencing in FXS human ESCs as reported by Colak et al. (2014) is indicated and no significant drop of *FMR1* mRNA expression is observed before or after this time in any line. Black circles next to each line indicate mean percentage of DNA methylation across 22 CpGs of the *FMR1* promoter at day 90 of differentiation. Data points represent mean of three independent differentiations ± SEM. See also Figure S5.

(B) Antibody staining of FMRP, the protein product of *FMR1*, in iPSC-derived neurons at day 60 of neuronal differentiation. FMRP, red; DAPI, blue. Except for the UFM1-11 clone with fully methylated and silent *FMR1*, FMRP was detected in all clones. Scale bar, 20 μm.

FMR1. Consistently, we did not find any mutation common to the two UFMs that would obviously impair the silencing machinery (Figure S4A; Tables S2 and S3). Neither did we identify a common mutation in the proximal regulatory sequences of *FMR1* (Figures S4B–S4D).

FMR1 Silencing Status Is Not Affected by Differentiation of UFM iPSC Clones

The conversion of an active UFM allele to a silenced one required an increase of the CGG repeat length. However, switching from an active to a silenced state, without changes in the repeat size, underlies the process of developmental silencing of *FMR1* in FXS embryos and has been modeled by neuronal differentiation of FXS human ESCs (Colak et al., 2014; Eiges et al., 2007; Sutcliffe et al., 1992; Telias et al., 2013). Therefore, we evaluated the stability of *FMR1* expression during neuronal differentiation of UFM iPSCs.

The exact time window of *FMR1* silencing during in vitro differentiation of FXS human ESCs to cortical neurons has been reported at day 45 (Colak et al., 2014). We applied the same differentiation protocol to iPSCs from two UFM individuals with variable CGG repeat sizes and *FMR1* silencing status (Figure 5). We used four iPSC lines with unmethylated expanded repeats, namely UFM1-5 (320 CGG), UFM1-9 (420 CGG), UFM2-5 (200 CGG), and UFM2-9 (260 CGG), as well as iPSC clone UFM1-11 with methylated expanded repeats of 480 CGG. Two WT lines, either with UFM1 background (UFM1-1) or from an unrelated healthy donor 86-14, were used as controls. All lines were efficiently differentiated into class III β-tubulin/MAP2-positive neurons (Figure S5). We analyzed the expression level of *FMR1* mRNA at four time points, up to 90 days of neuronal differentiation (Figure 5A). At day 60 we additionally confirmed the presence of FMRP by immunofluorescence (Figure 5B). For all the lines with active *FMR1* we observed a gradual increase in the expression during differentiation (Figure 5A), consistent with the described dynamics of *FMR1* expression during neuronal differentiation of WT human ESC lines (Telias et al., 2013). We also did not detect the appearance of any methylated *FMR1* alleles at day 90 (Figure 5A). No major changes in the size of the CGG repeats were found at this time point (data not shown). Also the methylation status of clone UFM1-9, which had 8% of its alleles methylated in the iPSC state, did not change during differentiation into neurons (7%–10% in three independent differentiations). In addition, line UFM1-11, with the longest CGG repeat size (480), retained full methylation of the *FMR1* promoter.

We conclude that the silencing status of *FMR1* is a stable feature of a given repeat size in the UFM background. Furthermore, this result shows that UFM cells are not subjected to developmental silencing induced by neuronal differentiation.

iPSC-Derived Neurons from UFM Subjects Show Phenotypic Properties of FXTAS

Ubiquitin-positive inclusion bodies (IBs) are found in postmortem brain samples of FXTAS patients (Greco et al., 2006) and in mouse models of FXTAS (Wenzel et al., 2010) expressing the *FMR1* with repeat sizes between 50 and 200 CGG. Therefore, to analyze the phenotypic

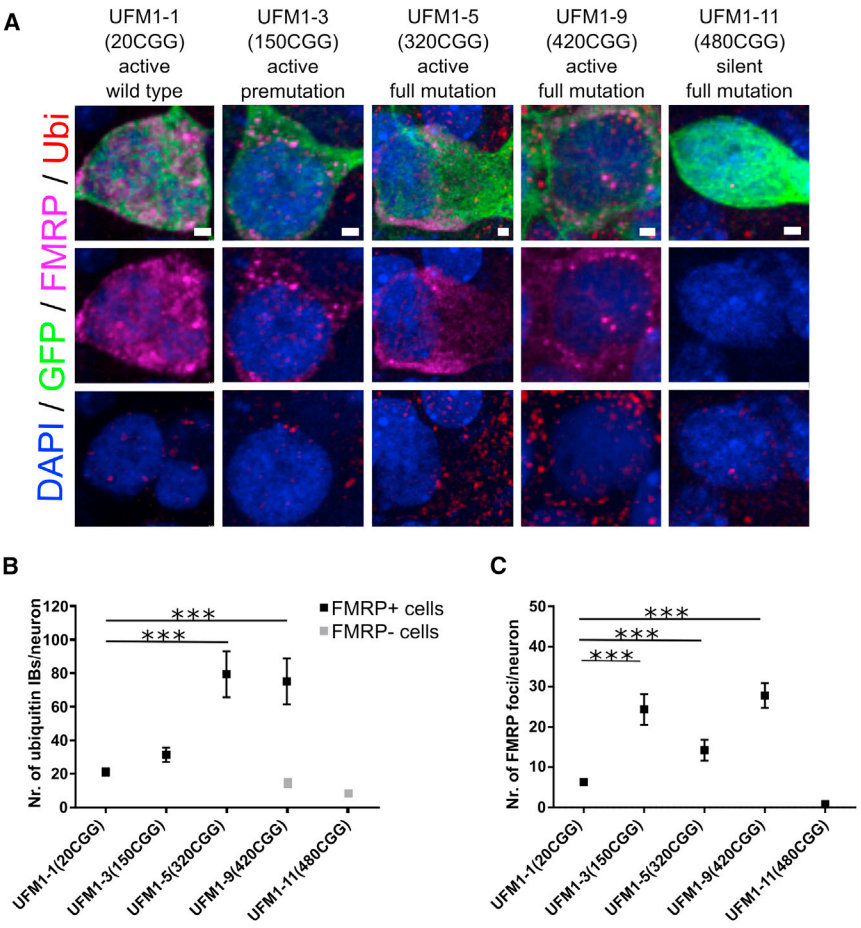

Figure 6. Neurodegenerative Features of UFM iPSC-Derived Neurons

(A) Representative images of staining for ubiquitin and FMRP inside GFP-labeled, isogenic, iPSC-derived neurons with spectrum of CGG repeat sizes corresponding to WT (UFM1-1), classical premutation (UFM1-3), UFM (UFM1-5 and UFM1-9), and FXS (UFM1-11). The iPSC-derived neurons were cultured within murine brain slices for 6 weeks. Ubiquitin (Ubi), red; FMRP, magenta; GFP, green; DAPI, blue. Multiple ubiquitin-positive inclusion bodies (IBs) are detected in UFM lines UFM1-5 and UFM1-9. Punctuated staining of FMRP is observed in UFM1-3, UFM1-5, and UFM1-9. Scale bars, 2 μm.

(B) Number of ubiquitin IBs per cell body of GFP-labeled human neuron. IBs ≥0.5 μm were counted. Black and gray bars represent FMRP-positive and -negative cells, respectively. Increased number of IBs is observed in both UFM clones but only for cells expressing FMRP. n = 15–50 cells per line coming from three independent rounds of brain slice injections (three mice). Data are presented as mean ± SEM; ***p < 0.0001, unpaired Student's t test.

(C) Number of FMRP foci per cell body of GFP-labeled human neuron. FMRP foci ≥0.5 μm were counted. For UFM1-9 only cells expressing FMRP are quantified. n = 15–50 cells per line coming from three independent rounds of brain slice injections (three mice). Data are presented as mean ± SEM; ***p < 0.0001, unpaired Student's t test.

consequences of the expression of *FMR1* with more than 200 repeats, we analyzed the numbers of ubiquitin-positive IBs in UFM iPSC-derived neurons (Figure 6). To enhance the maturation of neuronal precursors we used a co-culture system, whereby iPSC-derived neuronal progenitors are transiently transfected with a GFP expression vector and injected into organotypic mouse brain slices (OTBS) containing cortex, striatum, and hippocampus (Pecho-Vrieseling et al., 2014). After 6 weeks of co-culture we compared the number of ubiquitin IBs in isogenic iPSC-derived neurons only differing in the repeat size. UFM1-5 (320 CGG) and UFM1-9 (420 CGG), which expressed *FMR1*, were evaluated for the FXTAS phenotype whereas UFM1-1 (20 CGG), UFM1-3 (150 CGG), and UFM1-11 (480 CGG) with silenced *FMR1* served as WT, premutation, and FXS controls, respectively (Figure 2). We found multiple ubiquitin inclusions throughout the cell bodies of GFP-positive human neurons (Figures 6A and 6B). We quantified the number of inclusions in both cytoplasm and nucleus and found significantly higher numbers in the UFM clone (UFM1-5) compared with WT (UFM1-1) (Figures 6A and 6B). This effect was not observed for premutation (UFM1-3) neurons, indicating that expression of mRNA with 150 CGG repeats is not sufficient to trigger the effect. All the quantified cells in clones UFM1-1, UFM1-3, and UFM1-5 expressed *FMR1* as judged from FMRP staining. For UFM clone UFM1-9 with 8% methylated alleles we observed that only a proportion of neurons expressed FMRP and found a significantly higher number of inclusions only in these cells. The proportion of neurons that did not express FMRP did not show this effect, similar to neurons from FXS clone UFM1-11 with fully methylated *FMR1* (Figures 6A and 6B). Thus, expression of *FMR1* with expanded repeat is required for the accumulation of ubiquitin IBs.

In addition, we observed a dotted, aggregate-like pattern of FMRP staining in neurons derived from premutation (UFM1-3) and both UFM clones (UFM1-5 and UFM1-9) compared with an even distribution of FMRP in WT (UFM1-1) neurons (Figures 6A and 6C). We quantified the

number of these FMRP aggregate-like structures in neuronal cell bodies and found a significant increase in premutation and UFM neurons compared with WT (Figure 6C). As expected, no FMRP staining was observed in FXS (UFM1-11) neurons.

These data together suggest that UFM neurons may develop FXTAS neurodegenerative pathology. Moreover, some pathological phenotypes were only present or more pronounced in UFM when being compared with premutation neurons.

DISCUSSION

Genotype-phenotype correlation is greatly affected by inter-individual genetic differences and external factors. This variability is particularly relevant for the penetrance of genetic variants and may explain the spectrum of clinical phenotypes. In extreme cases, individuals who carry a pathological mutation may lack disease features. Dissecting the correlation between genotype and phenotype in these individuals may provide novel insights into the disease.

FXS is caused by a CGG trinucleotide repeat expansion in the 5′ UTR of *FMR1* that leads to its developmental silencing. There is a broadly accepted consensus that 200 CGGs represent the threshold above which the *FMR1* promoter becomes methylated and its transcription is turned off (Biancalana et al., 2015; Willemsen et al., 2011). An exception to this rule has been identified in rare UFM individuals who do not silence *FMR1* despite the expansion above this threshold (Smeets et al., 1995; Tabolacci et al., 2008; Wohrle et al., 1998). Whether these individuals have lost the capacity to silence *FMR1* locus has so far remained elusive.

In this study, we demonstrate that in two unrelated UFM cases *FMR1* silencing is not completely impaired. However, we found that the CGG repeat number necessary to trigger silencing is around 400 CGG rather than 200 CGG described for FXS patients. Analysis of iPSC clones with a spectrum of discrete repeat sizes allowed us to dissect the relation of CGG repeats with the silencing status of *FMR1*, previously only evaluated in primary cells and tissues with complex mosaic patterns of CGG repeat lengths. We show that in the majority of iPSC clones derived from the two UFM subjects, the *FMR1* promoter was unmethylated and active (Figure 2). In contrast, clones from FXS subject F-N1 in majority were silenced (Figure 3). However, also in a fraction of UFM clones with more than 400 CGG repeats *FMR1* was methylated and not expressed. An exception to this was the methylated clone UFM1-4 with 180 CGG repeats. It is not fully exceptional for a high premutation to be methylated, although very infrequent (Rousseau et al., 1994; G.N., unpublished data). Moreover, we detected ~5% methylated alleles in blood of both UFMs, indicating that silencing of *FMR1* in UFM background is not an artifact of iPSCs but occurs in vivo as well (Figure 1C).

To test whether UFM iPSCs are capable of de novo methylation and silencing of *FMR1*, we applied a selection pressure paradigm to unmethylated expanded alleles (Figure 4). Indeed, we found very rare events of methylation gain that were associated with a major increase in the number of CGG repeats. This demonstrates that UFM iPSCs are capable of gaining DNA methylation at the *FMR1* promoter when the CGG size is higher than their silencing threshold. By using a reporter knocked into the *FMR1* gene we monitored the silencing events in the endogenous locus that allowed us to evaluate if both *cis* and *trans* components of silencing machinery are in place in UFM cells. This is especially relevant, as the CGG-mediated silencing of *FMR1* has not been recapitulated in the transient transfection or randomly integrated reporter assays (Solvsten and Nielsen, 2011). The result of our experiment suggests that UFM individuals possess all the necessary components for the silencing of *FMR1*. Consistent with this notion, we have not identified any obvious genetic mutation common to both UFM individuals by analyzing the exome sequence of components of the epigenetic machinery and the regulatory sequences of the *FMR1* locus, including the sequence of the CGG repeat implicated in silencing initiation (Colak et al., 2014) (Figure S4).

Little is known about why the silencing threshold lies at 200 CGG repeats in FXS. In human ESCs carrying unmethylated CGG expansions a formation of a DNA:RNA hybrid over the CGG repeat is required for silencing initiation (Colak et al., 2014). Recently the direct dependence of *FMR1* silencing maintenance on the expanded CGG repeat has been demonstrated by removal of the repeat with CRISPR/Cas9 in FXS iPSCs, which resulted in demethylation and reactivation of the *FMR1* (Park et al., 2015). Here, by using a selection strategy we demonstrate that by increasing the length of the repeat an active *FMR1* allele becomes silenced and furthermore that it can be reverted to an active state upon a contraction event (Figure 4). Therefore, the dependence of the *FMR1* activity on the repeat length is bidirectional. Our selection system provides a tool to further study the dynamics of *FMR1* silencing.

The *FMR1* gene with more than 200 CGG repeats is silenced during early embryonic development (Sutcliffe et al., 1992). This process has been modeled in human ESCs derived from embryos carrying the *FMR1* full mutation. In these cells *FMR1* is silenced during in vitro neuronal differentiation (Colak et al., 2014; Eiges et al., 2007; Telias et al., 2013). Unfortunately, it is not possible to obtain human ESCs from UFM individuals. However, a

recent study suggests that there is genetic and epigenetic equivalence of human ESCs and iPSCs with matched genetic background (Choi et al., 2015). Therefore, we investigated whether UFM iPSC clones with a spectrum of unmethylated repeat lengths would silence *FMR1* in this developmental model (Figure 5). We neither observed a drop in the expression nor an appearance of methylated alleles at all analyzed stages of neuronal differentiation. Additionally, the silenced methylated status of cells with more than 450 CGG repeats did not change. These data suggest that the activity status of an allele with a given repeat size is maintained in iPSC-derived neurons. Furthermore, the expanded unmethylated alleles are resistant to silencing during differentiation. If the lack of methylation in UFM was a result of a maternal effect or stochastic events, *FMR1* would have been silenced during in vitro differentiation as observed in human ESCs carrying the *FMR1* full mutation (Colak et al., 2014; Eiges et al., 2007; Telias et al., 2013). However, our data suggest that the UFM cells possess intrinsic properties that affect their silencing threshold causing the lack of *FMR1* methylation during neuronal differentiation.

Recently, iPSCs were derived from fibroblasts obtained from another unrelated UFM subject (de Esch et al., 2014). The lymphoblastoid cell line from this subject has been previously characterized and showed the same epigenetic profile of the *FMR1* promoter-like lymphoblastoid cells from UFM1 (Pietrobono et al., 2005; Tabolacci et al., 2008). However, the authors reported that upon iPSC derivation the *FMR1* promoter gained methylation and the *FMR1* expression was shut off in all derived clones (de Esch et al., 2014). Inter-individual heterogeneity of the UFM group may be the cause of different results of UFM reprogramming in our study. Alternatively, different sources of the material being fibroblasts and PBMCs in de Esch et al. (2014) in their two respective studies may have led to this discrepancy. However, we reproduced the results of Avitzour et al. (2014) obtaining a UFM-like clone from an independent FXS fibroblast line (GM09497, Figure 3), which suggest that different cell type origins alone would not result in clones with different silencing status. Furthermore, the results from de Esch et al. (2014) are in agreement with our observation that UFM subjects retain the ability to silence *FMR1*. In addition, the published data may well be interpreted in favor of an altered silencing threshold. The fibroblasts used by de Esch et al. (2014) for reprogramming carried the repeat sizes of 200–230 CGGs. The CGG size disclosed for two silent iPSC clones in de Esch et al. (2014) were 330 and 380 repeats. The difference between the original repeat size of the fibroblasts and the one reported in the iPSC clones with silent *FMR1* is in line with our hypothesis of a shifted silencing threshold in UFM individuals.

Our observation of the variability in the silencing threshold is not limited to the UFM group, as we also detected this phenomenon in FXS patients. From a UFM-related FXS subject F-N1 and from an unrelated patient, FX97 (derived from GM09497 fibroblasts), we derived iPSC clones (Figure 3). All clones from both individuals carried *FMR1* alleles with more than 200 CGG repeats, most of them being silenced as previously described for FXS iPSCs (Sheridan et al., 2011; Urbach et al., 2010). However, some of the clones were active, hypomethylated, and had lower CGG repeat sizes than the silenced ones, consistent with a shift in the *FMR1* silencing threshold in these cells. Interestingly, in a recent report iPSCs were derived from the same fibroblasts GM09497 (Avitzour et al., 2014). Among four clones one was carrying an active *FMR1* allele with a fully expanded repeat, while the remaining three were silenced. The exact repeat size of the clones is not reported. Nevertheless, these data show the reproducibility of our results and indicate that the shift in the repeat threshold is an intrinsic property of the cells and not a random phenomenon. Our data support the hypothesis that the number of CGG repeats that triggers the epigenetic silencing of the *FMR1* promoter may vary between individuals.

In our model, the persistence of the increased silencing threshold in UFM iPSC-derived neurons prevents the development of the FXS phenotype. However, the expressed expanded CGG repeat is predicted to give rise to an additional phenotype in these neurons. Individuals that carry active *FMR1* alleles with 50–200 CGG repeats (permutation) are at risk of developing the late-onset neurodegenerative disease FXTAS, and there have been reports of FXTAS diagnosis in UFM individuals (Basuta et al., 2015; Loesch et al., 2012). Key hallmarks of this disease are relatively large, single per cell, intra-nuclear ubiquitin-positive IBs found in postmortem brain samples from FXTAS patients as well as in mouse models (Greco et al., 2006; Wenzel et al., 2010). At the cellular level FXTAS phenotype has been explored in iPSCs from a premutation individual carrying an expansion of 94 CGG repeats (Liu et al., 2012). However, the authors did not report on the presence of ubiquitin IBs. In the FXTAS brain samples a correlation of the CGG repeat number and the percentage of neurons with IBs has been observed (Greco et al., 2006). Therefore, iPSCs that express *FMR1* mRNA with more than 200 CGG repeats may potentially show enhanced or accelerated FXTAS phenotypes. Indeed, we find that neurons carrying more than 200 CGG repeats showed significantly increased numbers of ubiquitin-positive IBs compared with WT neurons (Figure 6B). This effect was not present in cells with silenced *FMR1* as judged by FMRP staining, indicating that not the expansion per se but the expression of the expended repeat is necessary to trigger the effect.

We did not observe an increased number of ubiquitin IBs in neurons derived from an isogenic iPSC line with a classical premutation length. It is likely that the expression of mRNA with longer CGG repeat lengths in UFM neurons results in accelerated pathological development compared with premutation neurons. Furthermore, in contrast to a single large intra-nuclear IB observed in FXTAS mouse models or in postmortem brain samples of FXTAS patients, we found multiple IBs in both cytoplasm and nucleus. The iPSC-derived neurons represent an early developmental stage in comparison with an aging brain. Developmental progression of the number and size of the inclusions is reported in FXTAS mice (Wenzel et al., 2010). Therefore, the pattern of ubiquitin inclusions observed here may reflect an early stage of the IB formation at the onset of the disease. Additionally we detected that both premutation and UFM neurons show increased numbers of FMRP aggregate-like structures (Figure 6C). FMRP has been reported to have a tendency to aggregate and spontaneously misfold toward β-rich structures in vitro (Sjekloca et al., 2011). Therefore, aggregation of FMRP may be contributing to the FXTAS pathology. Overall, our data provide evidence for an increased accumulation of ubiquitin and FMRP inclusions in UFM iPSC-derived neurons, which may be signs of an accelerated FXTAS phenotype in the UFM lines compared with the classical premutation.

In summary, our analyses reveal that UFM individuals have not lost the ability to silence *FMR1*, but the size of the CGG expansion triggering the silencing is higher than the one described in FXS patients (200 CGG). Furthermore, inter-individual variability in the CGG size requited for silencing is present not only in UFM but also in two FXS patients analyzed in this study. We propose a model in which the threshold size together with the proportion of the *FMR1* alleles below this threshold delineates UFM and FXS phenotypes. UFM do not silence *FMR1* and are spare of FXS pathology; nevertheless, our data suggest that the expression of *FMR1* gene with large CGG expansion may increase their risk of developing FXTAS.

EXPERIMENTAL PROCEDURES

Ethics and Sample Collection

The sample collection and all of the Experimental Procedures were approved by the Ethics committees of the Catholic University School of Medicine in Rome and the Ethikkommission Nordwest- und Zentralschweiz. Proper informed consent was obtained from all donors. Blood samples were collected from UFM individuals, their healthy brothers, and FXS nephew of UFM1. Buccal swab samples were obtained from additional family members. Primary skin fibroblasts GM09497 were obtained from Coriell Institute for Medical Research. Experiments involving mice were carried out in accordance with authorization guidelines of the Swiss Federal and Cantonal veterinary offices for care and use of laboratory animals and were approved by the Swiss Cantonal veterinary office and performed according to Novartis animal license number 2063.

FMR1 DNA Methylation, CGG Repeat Length, and Expression

CGG repeat number in the 5′ UTR of *FMR1* was analyzed by PCR amplification using an AmplideX FMR1 PCR kit (Asuragen) and agarose gel electrophoresis if not stated differently. DNA methylation of 22 CpGs of the *FMR1* promoter was analyzed using bisulfite pyrosequencing by EpigenDx. Expression of *FMR1* was quantified using TaqMan assay Hs00924547_m1 (Thermo Fisher). See Supplemental Experimental Procedures for the details.

iPSC Derivation and Neuronal Differentiation

iPSCs were derived from activated T cells isolated from PBMCs using a CytoTune-iPS Reprogramming Kit (Invitrogen). iPSCs were cultured on Matrigel (Corning) in mTeSR medium (Stem Cell Technologies) or Nutristem (Biological Industries). iPSCs were differentiated to neurons using the dual SMAD inhibition protocol (Chambers et al., 2009). Neuronal precursor cells derived from iPSCs were differentiated either on Matrigel or on OTBS using a previously described method (Pecho-Vrieseling et al., 2014). For detailed iPSC derivation and differentiation protocols, see Supplemental Experimental Procedures. The iPSC lines generated in this study are available upon request for research to study FXS and related diseases if all legal and ethical standards are met.

Immunostaining and Image Analysis

Immunostaining was performed using standard procedures explained in detail in Supplemental Experimental Procedures, using the following antibodies: rabbit anti-class III β-tubulin (PRB-435P, BioLegend), chicken anti-MAP2 (ab5392, Abcam), mouse anti-FMRP (Sc-101048, Santa Cruz Biotechnology), and rabbit anti-ubiquitin clone 10H4L21 (701339, Thermo Fisher). Images were acquired with a Zeiss confocal microscope. Ubiquitin and FMRP spots lying within the GFP-positive human neurons were counted manually using visualization with Imaris software as described in Supplemental Experimental Procedures.

Thymidine Kinase Knockin and Positive-Negative Selection

A P2a peptide-hygromycin-HSV thymidine kinase-stop codon-SV40 poly(A)(Hyg-TK) cassette was inserted into exon 4 of *FMR1* using CRISPR-mediated homologous recombination. For the details of construct generation, validation, and selection procedure, see Supplemental Experimental Procedures. Knockin lines were maintained in Nutristem medium (Biological Industries) supplemented with 25 μg/mL hygromycin. Positive-negative selection was performed with 10 μM ganciclovir without hygromycin.

Exome Sequencing, *FMR1* Promoter, and CGG Sequencing

Details of exome sequencing, Sanger sequencing of *FMR1* promoter, and single-molecule real-time sequencing (SMRT) of the

CGG repeat tract are described in Supplemental Experimental Procedures.

Statistical Analysis

Statistical analysis in Figure 6 was performed with Prism (Graphpad) software. The unpaired Student's t test was used to determine significant differences between groups. Random samples from each mouse were taken. No mice and data points were excluded from the analysis. OTBSs that showed a severe degeneration of both hemispheres (measured as holes in the cultures) were excluded from the analysis.

ACCESSION NUMBERS

Exome sequencing data have been deposited at the European Genome-Phenome Archive (EGA, https://ega-archive.org), under accession number EGAS00001001737. The data are accessible to the FXS research community via the controlled access procedure of the EGA.

SUPPLEMENTAL INFORMATION

Supplemental Information includes Supplemental Experimental Procedures, five figures, and three tables and can be found with this article online at http://dx.doi.org/10.1016/j.stemcr.2016.10.004.

AUTHOR CONTRIBUTIONS

U.B., E.P.-V., M.M., B.G.M., G.R., E.J.O., M. Buehler, P.C., G.N., T.B., F.P.d.G., and B.D.F. designed the experiments; U.B., E.P.-V., A.T., J.K., I.F., S.F., T.D., C.M., M.I., U.N., and E.T. performed the experiments; U.B., M. Beibel, N.K., and B.D.F. performed the NGS data analysis; U.B., F.P.D., and B.D.F. wrote the manuscript with input from T.B., M. Buehler, E.P.-V., G.N., E.T., and G.R.

ACKNOWLEDGMENTS

We thank Kathrin Wagner, Daniel Kaiser, and Andreas Katopodis from Novartis Institutes for Biomedical Research (NIBR) for purification of PBMCs and isolation of T cells. We thank Shola Richards, Ieuan Clay, Caroline Gubser Keller, Sarah Brasa, Remi Terranova, and Ivan Galimberti from NIBR for discussions on data analysis and interpretation. We thank Yi Yang from NIBR for Cas9-gRNA vector. We thank Stephen Helliwell for comments on the manuscript. Research in the E.T., P.C., and G.N. laboratories was funded by Telethon grant to E.T. (GGP15257A).

Received: April 7, 2016
Revised: October 11, 2016
Accepted: October 13, 2016
Published: November 10, 2016

REFERENCES

Avitzour, M., Mor-Shaked, H., Yanovsky-Dagan, S., Aharoni, S., Altarescu, G., Renbaum, P., Eldar-Geva, T., Schonberger, O., Levy-Lahad, E., Epsztejn-Litman, S., et al. (2014). FMR1 epigenetic silencing commonly occurs in undifferentiated fragile X-affected embryonic stem cells. Stem Cell Rep. *3*, 699–706.

Basuta, K., Schneider, A., Gane, L., Polussa, J., Woodruff, B., Pretto, D., Hagerman, R., and Tassone, F. (2015). High functioning male with fragile X syndrome and fragile X-associated tremor/ataxia syndrome. Am. J. Med. Genet. A *167A*, 2154–2161.

Biancalana, V., Glaeser, D., McQuaid, S., and Steinbach, P. (2015). EMQN best practice guidelines for the molecular genetic testing and reporting of fragile X syndrome and other fragile X-associated disorders. Eur. J. Hum. Genet. *23*, 417–425.

Chambers, S.M., Fasano, C.A., Papapetrou, E.P., Tomishima, M., Sadelain, M., and Studer, L. (2009). Highly efficient neural conversion of human ES and iPS cells by dual inhibition of SMAD signaling. Nat. Biotechnol. *27*, 275–280.

Choi, J., Lee, S., Mallard, W., Clement, K., Tagliazucchi, G.M., Lim, H., Choi, I.Y., Ferrari, F., Tsankov, A.M., Pop, R., et al. (2015). A comparison of genetically matched cell lines reveals the equivalence of human iPSCs and ESCs. Nat. Biotechnol. *33*, 1173–1181.

Colak, D., Zaninovic, N., Cohen, M.S., Rosenwaks, Z., Yang, W.Y., Gerhardt, J., Disney, M.D., and Jaffrey, S.R. (2014). Promoter-bound trinucleotide repeat mRNA drives epigenetic silencing in fragile X syndrome. Science *343*, 1002–1005.

de Esch, C.E., Ghazvini, M., Loos, F., Schelling-Kazaryan, N., Widagdo, W., Munshi, S.T., van der Wal, E., Douben, H., Gunhanlar, N., Kushner, S.A., et al. (2014). Epigenetic characterization of the FMR1 promoter in induced pluripotent stem cells from human fibroblasts carrying an unmethylated full mutation. Stem Cell Rep. *3*, 548–555.

Eiges, R., Urbach, A., Malcov, M., Frumkin, T., Schwartz, T., Amit, A., Yaron, Y., Eden, A., Yanuka, O., Benvenisty, N., et al. (2007). Developmental study of fragile X syndrome using human embryonic stem cells derived from preimplantation genetically diagnosed embryos. Cell Stem Cell *1*, 568–577.

Greco, C.M., Berman, R.F., Martin, R.M., Tassone, F., Schwartz, P.H., Chang, A., Trapp, B.D., Iwahashi, C., Brunberg, J., Grigsby, J., et al. (2006). Neuropathology of fragile X-associated tremor/ataxia syndrome (FXTAS). Brain *129*, 243–255.

Hagerman, R.J., Hull, C.E., Safanda, J.F., Carpenter, I., Staley, L.W., O'Connor, R.A., Seydel, C., Mazzocco, M.M., Snow, K., Thibodeau, S.N., et al. (1994). High functioning fragile X males: demonstration of an unmethylated fully expanded FMR-1 mutation associated with protein expression. Am. J. Med. Genet. *51*, 298–308.

Hagerman, R.J., Leehey, M., Heinrichs, W., Tassone, F., Wilson, R., Hills, J., Grigsby, J., Gage, B., and Hagerman, P.J. (2001). Intention tremor, parkinsonism, and generalized brain atrophy in male carriers of fragile X. Neurology *57*, 127–130.

Liu, J., Koscielska, K.A., Cao, Z., Hulsizer, S., Grace, N., Mitchell, G., Nacey, C., Githinji, J., McGee, J., Garcia-Arocena, D., et al. (2012). Signaling defects in iPSC-derived fragile X premutation neurons. Hum. Mol. Genet. *21*, 3795–3805.

Loesch, D.Z., Sherwell, S., Kinsella, G., Tassone, F., Taylor, A., Amor, D., Sung, S., and Evans, A. (2012). Fragile X-associated tremor/ataxia phenotype in a male carrier of unmethylated full mutation in the FMR1 gene. Clin. Genet. *82*, 88–92.

Park, C.Y., Halevy, T., Lee, D.R., Sung, J.J., Lee, J.S., Yanuka, O., Benvenisty, N., and Kim, D.W. (2015). Reversion of FMR1 methylation and silencing by editing the triplet repeats in fragile X iPSC-derived neurons. Cell Rep. *13*, 234–241.

Pecho-Vrieseling, E., Rieker, C., Fuchs, S., Bleckmann, D., Esposito, M.S., Botta, P., Goldstein, C., Bernhard, M., Galimberti, I., Muller, M., et al. (2014). Transneuronal propagation of mutant huntingtin contributes to non-cell autonomous pathology in neurons. Nat. Neurosci. *17*, 1064–1072.

Pietrobono, R., Tabolacci, E., Zalfa, F., Zito, I., Terracciano, A., Moscato, U., Bagni, C., Oostra, B., Chiurazzi, P., and Neri, G. (2005). Molecular dissection of the events leading to inactivation of the FMR1 gene. Hum. Mol. Genet. *14*, 267–277.

Rousseau, F., Heitz, D., Tarleton, J., MacPherson, J., Malmgren, H., Dahl, N., Barnicoat, A., Mathew, C., Mornet, E., Tejada, I., et al. (1994). A multicenter study on genotype-phenotype correlations in the fragile X syndrome, using direct diagnosis with probe StB12.3: the first 2,253 cases. Am. J. Hum. Genet. *55*, 225–237.

Sheridan, S.D., Theriault, K.M., Reis, S.A., Zhou, F., Madison, J.M., Daheron, L., Loring, J.F., and Haggarty, S.J. (2011). Epigenetic characterization of the FMR1 gene and aberrant neurodevelopment in human induced pluripotent stem cell models of fragile X syndrome. PLoS One *6*, e26203.

Sjekloca, L., Pauwels, K., and Pastore, A. (2011). On the aggregation properties of FMRP—a link with the FXTAS syndrome? FEBS J. *278*, 1912–1921.

Smeets, H.J., Smits, A.P., Verheij, C.E., Theelen, J.P., Willemsen, R., van de Burgt, I., Hoogeveen, A.T., Oosterwijk, J.C., and Oostra, B.A. (1995). Normal phenotype in two brothers with a full FMR1 mutation. Hum. Mol. Genet. *4*, 2103–2108.

Solvsten, C., and Nielsen, A.L. (2011). FMR1 CGG repeat lengths mediate different regulation of reporter gene expression in comparative transient and locus specific integration assays. Gene *486*, 15–22.

Sutcliffe, J.S., Nelson, D.L., Zhang, F., Pieretti, M., Caskey, C.T., Saxe, D., and Warren, S.T. (1992). DNA methylation represses FMR-1 transcription in fragile X syndrome. Hum. Mol. Genet. *1*, 397–400.

Tabolacci, E., Moscato, U., Zalfa, F., Bagni, C., Chiurazzi, P., and Neri, G. (2008). Epigenetic analysis reveals a euchromatic configuration in the FMR1 unmethylated full mutations. Eur. J. Hum. Genet. *16*, 1487–1498.

Takahashi, K., Tanabe, K., Ohnuki, M., Narita, M., Ichisaka, T., Tomoda, K., and Yamanaka, S. (2007). Induction of pluripotent stem cells from adult human fibroblasts by defined factors. Cell *131*, 861–872.

Telias, M., Segal, M., and Ben-Yosef, D. (2013). Neural differentiation of Fragile X human Embryonic Stem Cells reveals abnormal patterns of development despite successful neurogenesis. Dev. Biol. *374*, 32–45.

Urbach, A., Bar-Nur, O., Daley, G.Q., and Benvenisty, N. (2010). Differential modeling of fragile X syndrome by human embryonic stem cells and induced pluripotent stem cells. Cell Stem Cell *6*, 407–411.

Verkerk, A.J., Pieretti, M., Sutcliffe, J.S., Fu, Y.H., Kuhl, D.P., Pizzuti, A., Reiner, O., Richards, S., Victoria, M.F., Zhang, F.P., et al. (1991). Identification of a gene (FMR-1) containing a CGG repeat coincident with a breakpoint cluster region exhibiting length variation in fragile X syndrome. Cell *65*, 905–914.

Wenzel, H.J., Hunsaker, M.R., Greco, C.M., Willemsen, R., and Berman, R.F. (2010). Ubiquitin-positive intranuclear inclusions in neuronal and glial cells in a mouse model of the fragile X premutation. Brain Res. *1318*, 155–166.

Willemsen, R., Levenga, J., and Oostra, B.A. (2011). CGG repeat in the FMR1 gene: size matters. Clin. Genet. *80*, 214–225.

Wohrle, D., Salat, U., Glaser, D., Mucke, J., Meisel-Stosiek, M., Schindler, D., Vogel, W., and Steinbach, P. (1998). Unusual mutations in high functioning fragile X males: apparent instability of expanded unmethylated CGG repeats. J. Med. Genet. *35*, 103–111.

Stem Cell Reports, Volume *7*

Supplemental Information

CGG Repeat-Induced *FMR1* Silencing Depends on the Expansion Size in Human iPSCs and Neurons Carrying Unmethylated Full Mutations

Urszula Brykczynska, Eline Pecho-Vrieseling, Anke Thiemeyer, Jessica Klein, Isabelle Fruh, Thierry Doll, Carole Manneville, Sascha Fuchs, Mariavittoria Iazeolla, Martin Beibel, Guglielmo Roma, Ulrike Naumann, Nicholas Kelley, Edward J. Oakeley, Matthias Mueller, Baltazar Gomez-Mancilla, Marc Bühler, Elisabetta Tabolacci, Pietro Chiurazzi, Giovanni Neri, Tewis Bouwmeester, Francesco Paolo Di Giorgio, and Barna D. Fodor

Brykczynska et al., Figure S1

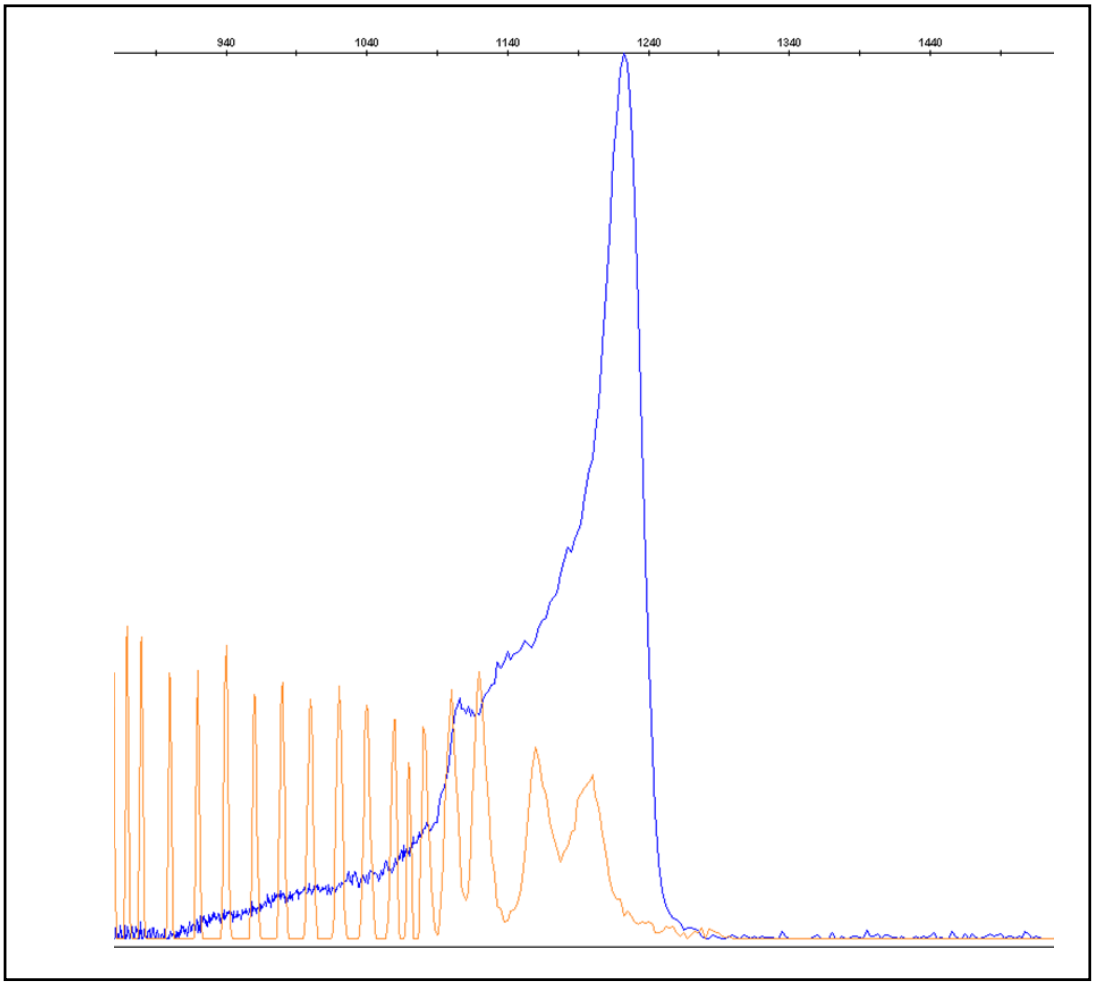

Brykczynska et al., Figure S2

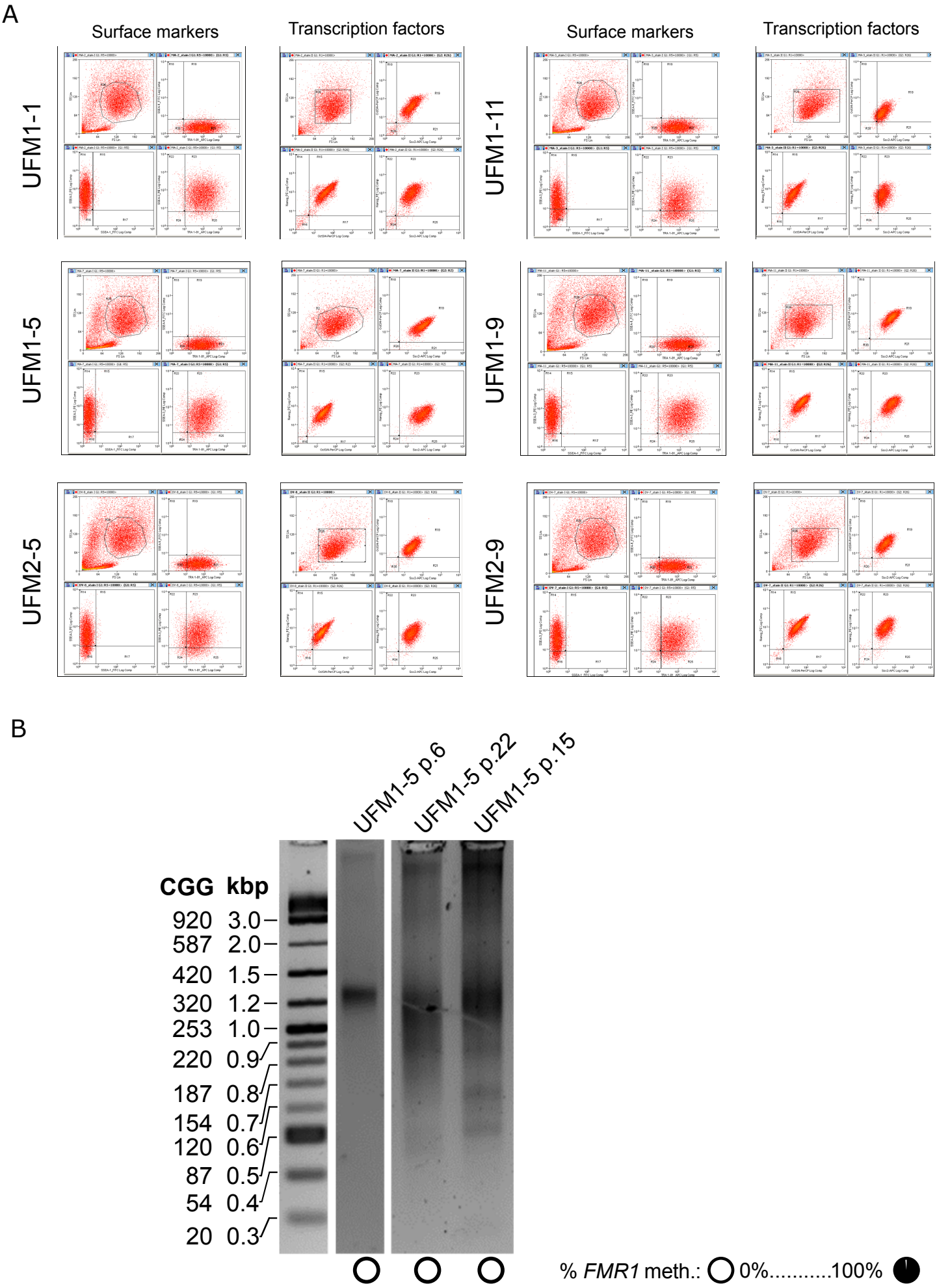

Brykczynska et al., Figure S3

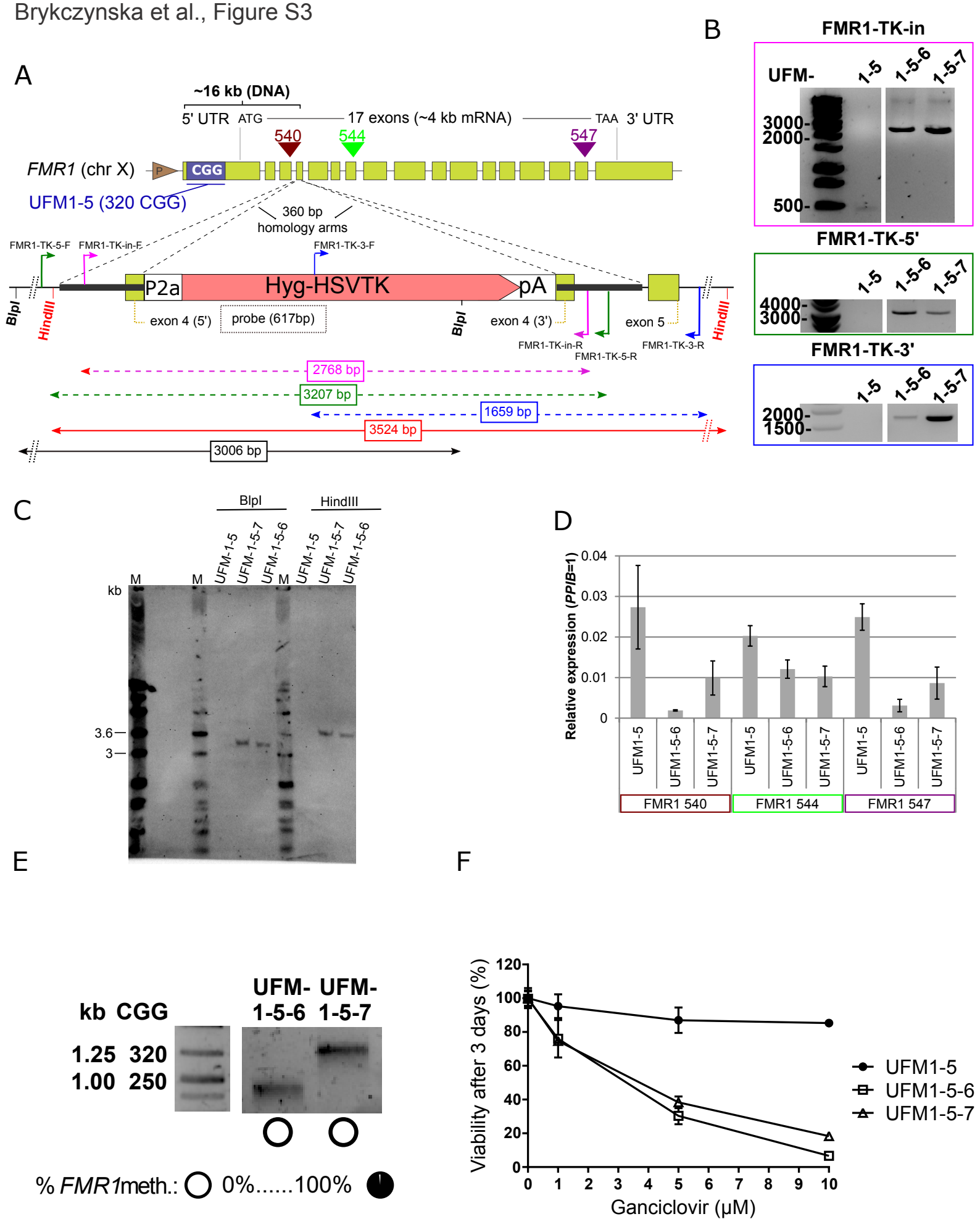

Brykczynska et al., Figure S4

A

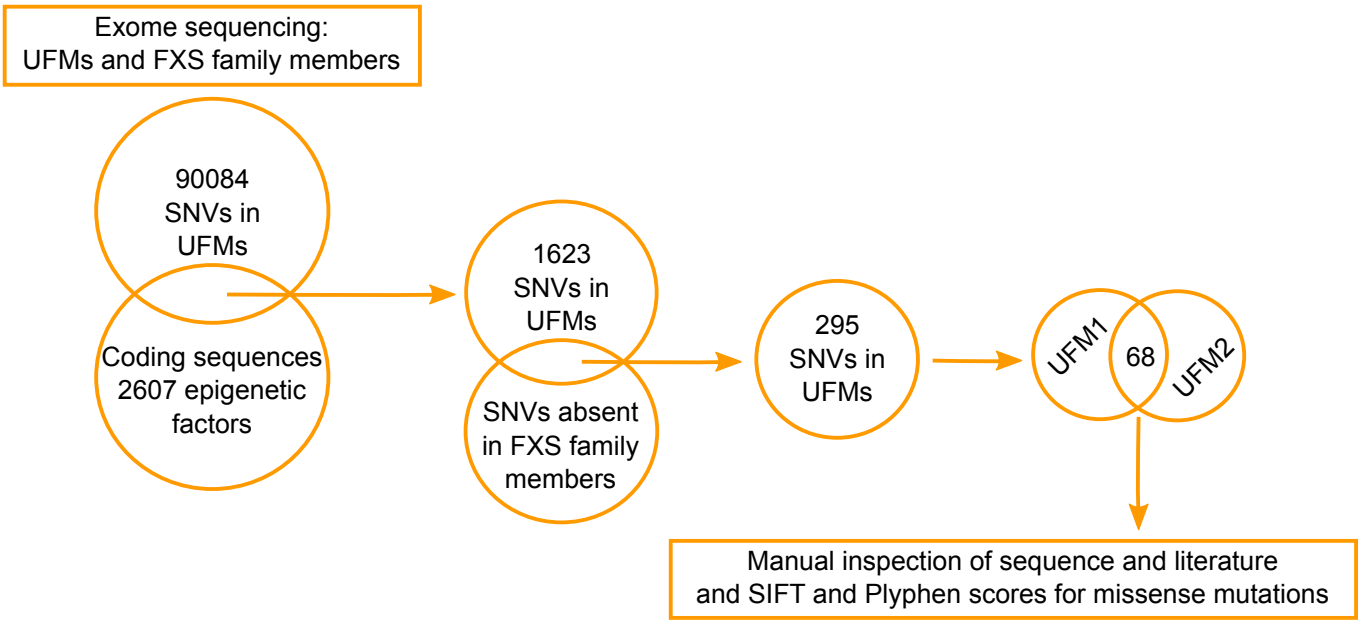

B

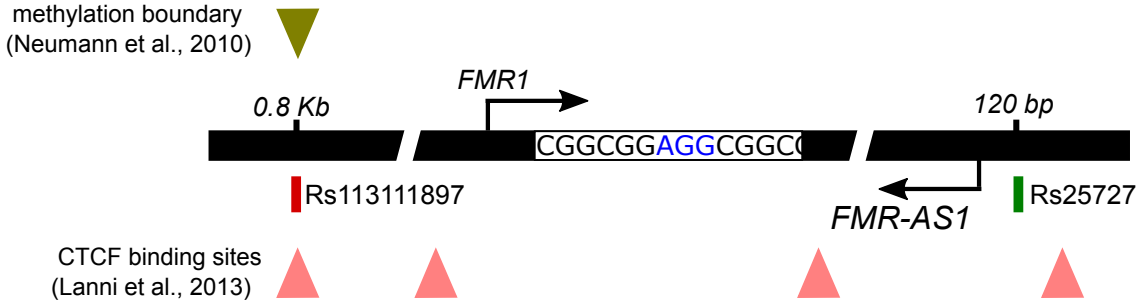

C

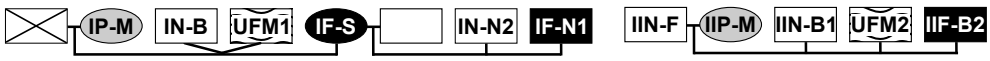

Rs113111897	G/A	G	A	G/A	G	A	G	G/G	G	G	G
Rs25727	NA	T	T	NA	NA	T	NA	NA	T	C	C
AGG position	9/19	9/19	10*	8	5/14	10*	9/19	9/19	9/19	0*	0

D

UFM1-5 529 forward sequences

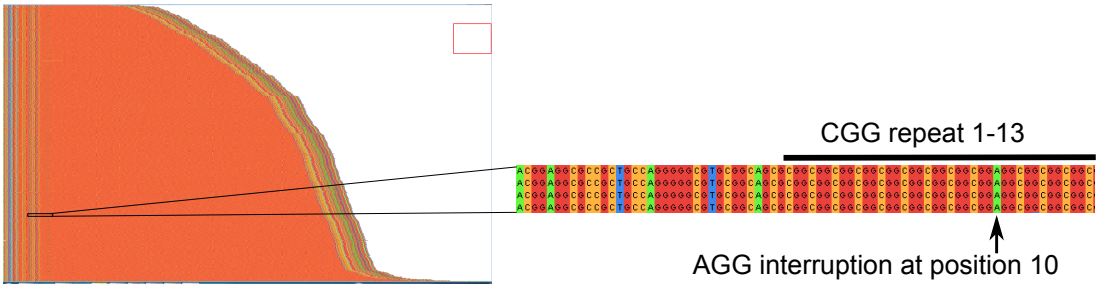

UFM2-7 742 forward sequences

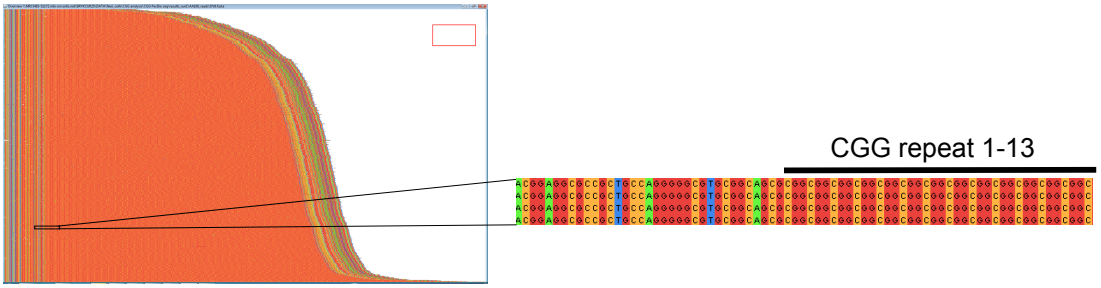

Brykczynska et al., Figure S5

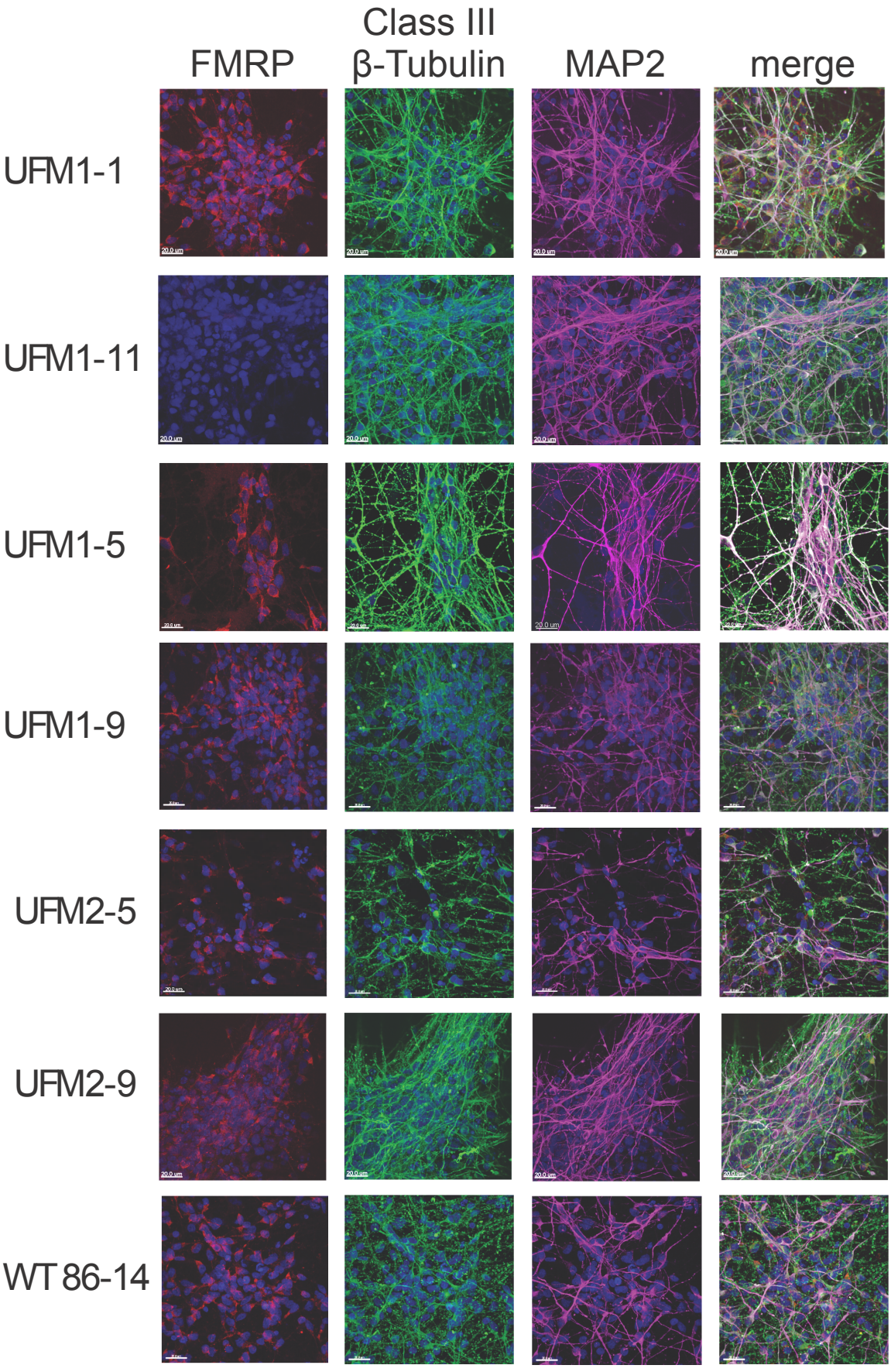

Supplemental Figure Legends

Figure S1. Related to Figure 1

Analysis of CGG expansion in UFM2

The electropherogram of the CGG triplet sequence (in blue) displays an expansion in the range of full mutation of around 280-330 triplets. The orange peaks are those of the 1200 LIZ dye size standard, the numbers in the upper part of the panel indicate the size of the run in bp.

Figure S2. Related to Figure 2 and Figure 3

Characterization of iPSC derived cells

A) Fluorescent-activated cell sorting (FACS) analysis of iPSC lines generated from T-cells of UFM individuals. Data for representative clones that were used in further experiments is shown. As expected majority of the cells are double positive for pluripotency surface markers SSEA-3 and TRA1-81 and negative for differentiation marker SSEA-1, as well as positive for pluripotency associated transcription factors NANOG, OCT4 and SOX2.

B) Stability of CGG repeat size and *FMR1* hypomethylation upon passaging of UFM iPSCs. PCR analysis of the CGG repeat size using Asuragen AmplideX FMR1 PCR kit followed by agarose gel electrophoresis for UFM1-5 iPSC clone at passage 6 and following two independent passaging to passage 22 and 15. Black circles under each lane indicate mean percentage of DNA methylation across 22 CpGs of the *FMR1* promoter based on data in Table S1. Certain instability of the CGG repeat is observed upon passaging but the unmethylated status of the *FMR1* promoter is not changed.

Figure S3. Related to Figure 4

Generation and characterization of the *FMR1* knock-in iPSC lines

A) Schematic representation of the *FMR1* knock-in strategy. Location of PCR primers used for validation of the correct integration is indicated with arrows and sizes of the expected PCR products between the arrows below. Similarly restriction sites of enzymes used for Southern blot analysis are indicated and sizes of the expected genomic fragments between the arrows below. Location of TaqMan probes used for evaluation of expression of *FMR1* after knock-in is indicated with triangles.

B) Validation of the correct cassette integration in two selected clones UFM1-5-6 and UFM1-5-7using PCR primers indicated in the scheme in panel (a) with sequences given in Supplementary Experimental Procedures. PCR primers FMR1-TK-in are spanning the homology arms. Cassette integration results in increase in the PCR product size from 495 bp in parental line UFM1-5 to 2768 bp in knock-in lines. PCR primers FMR1-TK-5 and FMR1-TK-3 are spanning the cassette and the 5' and 3' genomic regions respectively resulting in the 3207 bp product for FMR1-TK-5 and in 1659 bp products for FMR1-TK-3 when the cassette is integrated.

C) Southern blot confirming single integration of HyTK cassette into the genome. gDNA digested with BlpI and HindIII is loaded for parental line UFM1-5 and two selected clones UFM1-5-6 and UFM1-5-7. As expected single band is observed for two clones and no signal for the parental line. Band sizes correspond to the genomic DNA fragments of the *FMR1* locus with integrated HyTK cassette as indicated in panel A.

D) Expression of *FMR1* before (UFM1-5) and after the cassette integration (UFM1-5-6 and UFM1-5-7) based on TaqMan experiment with 3 probes located along the FMR1 mRNA as indicated in the scheme in panel A. Both knock-in clones express *FMR1* although at the reduced levels comparing to the parental line. Data are presented as a mean of three independent biological replicates. Error bars represent standard deviation.

E) CGG repeat size and *FMR1* promoter methylation in two knock-in clones UFM1-5-6 and UFM1-5-7. Black circles under each lane indicate mean percentage of DNA methylation across 22 CpGs of the *FMR1* promoter for a given clone based on data in Table S1.

F) Survival of parental line UFM1-5 and knock-in clones UFM1-5-6 and UFM1-5-7 with increasing amount of ganciclovir evaluated by Presto Blue fluorescence measurement (Thermo Fisher) after 3 days of treatment. Both subclones expressing Thymidine Kinase show lethality in 5-10 μM ganciclovir range in contrast to the parental line. Data are presented as a mean of three independent biological replicates. Error bars represent standard deviation.

Figure S4. Related to Figure 4

A) Filtering criteria for identification of a causative genetic variant common to two UFMs. To identify a common genetic cause of the UFM phenotype we performed exome-sequencing of UFM individuals and their family members. Strict filtering criteria were applied due to the small sample size. We only considered mutations affecting coding sequences of proteins broadly implicated in epigenetic processes. Further we filtered out the mutations present in FXS family members and considered mutations affecting the same gene in both UFMs. Among the 68 shortlisted candidates we haven't identified a mutation with obvious disrupting effect on the epigenetic machinery. This is in line with the fact that UFM cells retain the ability to silence *FMR1*. Furthermore, a dramatic impairment of the core epigenetic machinery would likely have strong consequences on the phenotype of UFM individuals.

B-D) Sequence analysis of *FMR1* and *FMR1-AS1* promoters and CGG repeat tract

B) Schematic representation of the *FMR1* locus with indicated SNPs detected in UFM individuals. Putative CTCF binding sites are indicated based on (Lanni et al., 2013) and the DNA methylation boundary based on (Naumann et al., 2009).

C) Presence and position of AGG interruptions in the CGG repeat tract and presence of SNPs in UFM individuals and their family members. AGG position was determined using Asuragen PCR kit and capillary electrophoresis allowing for analysis of the first 200 3'CGG repeats. For UFM1, UFM2 and F-N1 AGG (indicated by *) position was determined by PacBio single molecule sequencing (SMRT) allowing for evaluation of the entire repeat tract. The AGG position is given in number of CGG repeat units from the 5' end.

D) Representative images of multiple sequence alignment of CGG repeat amplicons sequenced with SMRT technology. 529 forward sequences of iPSC clone UFM1-5 and 742 forward sequences of UFM2-7 were aligned. AGG interruption at position 10 in UFM1-7 is highlighted. In all additional sequenced clones from UFM1 (UFM1-6, UFM1-9, UFM1-11 (silent FMR1)) and F-N1 (F-N1-3) the AGG interruption was detected at this position. No interruptions of the repeat tract were detected in sequenced UFM2 clones (UFM2-5 and UFM2-7).

Figure S5. Related to Figure 5

Characterization of iPSC derived neurons

FMRP (red), Class III β Tubulin (green), MAP2 (red) DAPI (blue) staining of iPSC derived neurons after 60 days of differentiation. Presence of FMRP (protein product of *FMR1*) is detected in all lines except UFM1-11 with 480 CGG repeats and silenced *FMR1*. MAP2 and -Class III β Tubulin staining indicates that at day 60 iPS cells were differentiated into post-mitotic neurons. Scale bar = 20μm

Supplemental Experimental Procedures

CGG repeat length analysis using PCR and gel electrophoresis

Genomic DNA from PBMCs, iPSCs and neurons was extracted using DNeasy kit (Qiagen). CGG repeat number and position of AGG was analyzed by PCR amplification using AmplideX FMR1 PCR kit (Asuragen) with with gel

electrophoresis as described previously (Filipovic-Sadic et al., 2010). Southern blot analysis of the CGG repeat size of UFM2 was performed as previously described (Tabolacci et al., 2008).

CGG repeat analysis using PCR and capillary electrophoresis in Fig. S1

The analysis of CGG-tract expansion in UFM2 peripheral blood lymphocytes' DNA was performed using FAM-fluorescent primers (CG-rich-F: TCA GGC GCT CAG CTC CGT TTC GGT TTC A and CG-rich-R: AAG CGC CAT TGG AGC CCC GCA CTT CC) and GC-rich PCR system (Roche, 12140306001). The PCR product was then separated on capillary electrophoresis on 3130 Genetic Analyzer (Life technologies) together with a 1200 LIZ dye size standard (4379950, Life technologies). The result was analyzed with Sequencing Analysis v5.2 software (Life technologies).

DNA methylation of *FMR1* promoter using bisulfite pyrosequencing

Genomic DNA from PBMCs, iPSCs and neurons was extracted using DNeasy kit (Qiagen). Bisulfite treatment and pyrosequencing analysis of the 22 CpGs of the *FMR1* promoter was performed by EpigenDx according to standard procedures with a unique set of primers that were developed by EpigenDx (assays ADS1451FS1 and ADS1451FS2).

Quantitative RT PCR for *FMR1*

RNA from iPSCs and neurons was extracted using RNeasy kit (Qiagen). Reverse transcription and amplification were performed using TaqMan Fast Virus 1-step reagent (Thermo Fisher) and Viaa7 real-time PCR System (Thermo Fisher). Pre-developed TaqMan assay was used for FMR1 (Hs00924547_m1) and PPIB (Hs00168719_m1) which was used for normalization of the *FMR1* signal.

iPSCs derivation

PBMCs were purified from blood samples using Lymphoprep density gradient (Axis-Shield). T cells were isolated from PBMCs using EasySep Human T Cell Enrichment Kit (Stem Cell technologies) according to kit instructions and activated using anti-CD3 antibody OKT-3 and IL-2 cytokine (Cedarlane) as previously described (Tsoukas et al., 1985). Activated T cells (or fibroblasts in case of GM09497) were transduced with Sendai viruses expressing Oct3/4, Sox2, Klf4, c-Myc (Takahashi et al., 2007) using CytoTune-iPS Reprogramming Kit (Invitrogen) according to kit instructions. 3 days after transduction cells were transferred onto mouse embryonic fibroblasts (CF1, Millipore) and cultured in iPSC medium containing 80% knockout Dulbecco's modified eagle medium (DMEM)/F12 (Gibco), 20% knockout serum replacement (Gibco), 10 ng/ml bFGF, 1 mM glutamax (Gibco), 0.1 mM b-mercaptoethanol (Gibco) and 1% non-essential amino acid solution (Gibco). After 3-4 weeks colonies with stem cell morphology were selected and manually passaged 5 times. After establishment, iPSCs were transferred into feeder free conditions on matrigel (Corning) and maintained in mTeSR medium (Stem Cell Technologies) with Pen/Strep supplement (Gibco). The absence of reprogramming vectors was confirmed using RT-PCR for Sendai virus expressed Oct3/4, Sox2, Klf4 and c-Myc as described in CytoTune-iPS Reprogramming Kit (Invitrogen). IPSC clones were analyzed between passage 5 and 10 for expression of pluripotency markers by Score card assay (Invitrogen) and for surface markers SSEA-3, TRA1-81 and SSEA-1 (negative marker), as well as pluripotency associated transcription factors NANOG, OCT4 and SOX2, using fluorochrome conjugated antibodies (BD Biosciences) and fluorescence activated cell sorting (FACS) using standard procedures.

Cell culture

iPSCs were cultured on matrigel in Nutristem (Biological Industries) or mTeSR1 (Stem Cell Technologies) medium, supplemented with Pen/Strep (Gibco). Cells were dissociated with TrypLE (Gibco) every 3-4 days, plated at the density of 10000/cm^2 for Nutristem or 20000/cm^2 for mTeSR in the presence of 10 μM ROCK inhibitor. The medium was replaced every day (mTeSR1) or every other day (Nutristem). Stable knock in clones with the Hyg-Tk cassette (UFM1-5-6 and UFM1-5-7) were maintained in Nutristem supplemented with 25 μg/ml hygromycin if not indicated differently. For positive-negative selection cells were plated at 10000-15000/cm^2 density and from next day on medium was supplemented with ganciclovir (10 μM) and with no hygromycin. For the first 3 days of

selection medium was changed every day and plates washed with PBS. Surviving subclones were picked and expanded in the presence of 10 μM ganciclovir (except the two first passages) and with no hygromycin. For the hygromycin selection of ganciclovir resistant clone UFM1-5-7-1, the clone was cultured without ganciclovir for 3 weeks and further with indicated concentrations of hygromycin for 7 days. Surviving colonies were picked and expanded in the presence of hygromycin.

Hygromycin-HSV-Thymidine Kinase knock-in into *FMR1*

To create an endogenous in frame fusion between a positive-negative selection marker and *FMR1* we designed a CRISPR mediated homologous recombination strategy targeting exon 4 of *FMR1* (Fig.4 and Fig. S3). The donor plasmid carried a P2a peptide-Hygromycin-HSV Thymidine Kinase-stop codon-SV40 polyA (Hyg-TK) cassette flanked by 360 bp homology arms. The Cas9-gRNA plasmid was a derivative of pU6-gRNA-SPycas9-2acherry (Smurnyy et al., 2014) and was generated by replacing the CMV promoter with the CBh promoter and removing the mCherry reporter (Yi Yang personal communication). The Cas9-gRNA plasmid was further modified by inserting a designed (http://crispr.mit.edu/) oligo encoding the 5'-ttagctaaccaccaacagca-3' gRNA sequence targeting *FMR1*. Cells were co-nucleofected with the donor and *FMR1* targeting Cas9-gRNA plasmid using Amaxa nucleofector (program B-016) with the Human Stem Cell Nucleofector Kit 1 (VPH-5012, Lonza). 72h after co-nucleofection cells were cultured in presence of 25 μg/ml hygromycin for 9 to 12 days. Single colonies were picked, subcloned and expanded. Selected subclones were further characterized to confirm the correct cassette integration by PCR (Fig. S3B). Primer sequences were FMR1-TK-in-F: 5'-TCAGAGCACTAATTATTGCTG-3'; FMR1-TK-in-R:5'-AAATTAGATATTACTTCAAAATAGA-3';FMR1-TK-5-F:5'GAGTATCCCTGTCTCTCTGTCCA-3'; FMR1-TK-5-R:5'-CAGAAACATACTGAACACATAGTG-3';FMR1-TK-3-F:5'-ACTCAACTGCTCGTAGCCCT -3' and FMR1-TK-3-R: 5'-GCAAACCAAACCATTTTTGC-3'. Two subclones UFM1-7-6 and UFM1-7-7 were selected for further experiments based on correct cassette integration, CGG repeat length, *FMR1* promoter methylation and mRNA expression (Fig. S3 B,D,E). In these two clones insertions of the HyTK cassette outside the *FMR1* locus was ruled out by Southern blot and hybridization on gDNA digested with BlpI and HindIII using the parental line as control. The DIG labeled probe was generated by PCR (Roche) using the primers oP3_for3: 5' ACGAAGTTGCCAACATTTTCTT 3' and oP3a_rev: 5' GGCATCCCCGGCACTAATCT 3' internal to the cassette (Fig. SC).

Neuronal differentiation iPSCs

iPSCs were differentiated into post mitotic neurons using dual SMAD inhibition protocol as previously described (Chambers et al., 2009) with modifications. Briefly, neuronal precursor cells (NPCs) were derived by seeding iPSCs into 96-well ultralow attachment plate (Costar) in neuronal induction medium (DMEM/F12 medium with GlutamaX (Gibco) supplemented with 20% Knockout-Serum Replacement (Gibco), 0.1mM MEM non-essential amino acids (Gibco), 0.1mM 2-Mercaptoethanol (Gibco), Pen/Strep supplement (Gibco), 10 ng/ml hFGF (Gibco), 10 μM SB 431542 (Stemgent) and 1 μM LDN 193189 (Stemgent)) with 10 μM ROCK inhibitor, at density 10 000 cells/well. The formed EBs were transferred after 3 days onto a matrigel coted plates and cultured in induction medium for additional 7 days. At day 10 of NPC derivation non-neuronal cells appearing at the edges of the attached EBs were manually scraped off, NPCs were detached (TrypLE, Gibco) and transferred onto matrigel coted dishes in proliferation medium (DMEM/F12 with Glutamax, supplemented with B27 and N2 (Gibco), Pen/Strep (Gibco), 10 ng/ml hEGF (Gibco), 10 ng/ml hFGF (Gibco)) with 10 μM ROCK inhibitor. NPCs were expanded in proliferation medium. For neuronal differentiation NPCs were seeded on matrigel plates with density: 250 000 cells/cm^2 and cultured in differentiation medium (Neurobasal Medium (Gibco), supplemented with B27 and N2 (Gibco), Pen/Strep supplement (Gibco), 10 ng/ml BDNF (R&D Systems), 10 ng/ml GDNF (R&D Systems), 10 ng/ml hNT3 (R&D Systems)) for the indicated number of days (indicated as number of differentiation days plus 10 days of NPC derivation). For immunofluorescence analysis NPCs were seeded and differentiated on glass slides coated with matrigel.

Differentiation of NPCs in organotypic mouse brain slices

NPCs derived from iPSCs were differentiated on organotypic mouse brain slices (OTBS) using a previously described method (Pecho-Vrieseling et al., 2014). Briefly, 400 μm thick coronal sections of brains of 5 days old pups were prepared using a vibratome (Leica). Slices containing striatum, cortex and hippocampus were selected and plated on Millicell inserts (Millipore). Slice cultures were maintained at 35 °C in a 5% CO_2/ 95% air atmosphere with a relative humidity 95% in OTBS medium (50% (vol/vol) MEM, 25 mM HEPES, 25% (vol/vol) HBSS, 25%

(vol/vol) heat-inactivated horse serum, 2 mM glutamine, 1 ml of penicillin/streptomycin solution and 0.044% (vol/vol) NaHCO3 adjusted to pH 7.2). IPSCs derived NPCs were labeled with GFP using CAG-GFP expression vector (Tchorz et al., 2012) nucleofected with Amaxa using basic nucleofector kit for primary neurons (Lonza). After nucleofection cells were resuspended in Neurobasal medium (Gibco) with 10 µM ROCK inhibitor at a concentration of 2×10^3 cells per µl and 0.5 µl of the cell suspension was injected into each brain slice hemisphere (30–45° angle), prepared 2 days before, using a Hamilton syringe (Hamilton). Co-cultures were further maintained as described above for slice cultures.

Immunostaining and image analysis

Cells and oragnotypic brain slices were fixed with 4% paraformaldehyde for 5min at 35°C for brain slices and at room temperature for cells, permeabilized and blocked in 0.1% (vol/vol) Triton-X100 (Sigma), 1% bovine serum albumin (Sigma) in PBS (blocking buffer). Staining was performed overnight at 4°C with the following primary antibodies diluted in blocking buffer: rabbit anti-Class III β-Tubulin (PRB-435P, BioLegend), chicken anti-MAP2 (ab5392, Abcam), mouse anti-FMRP (Sc-101048, Santa Cruz), rabbit anti-ubiquitin clone 10H4L21 (701339 Thermo Fisher). Appropriate fluorescence-labeled secondary antibodies were applied for 2h at room temperature, and nuclei were counterstained with 4′,6-diamidino-2-phenylindole (Sigma). Slides were mounted with ProLong Gold (Invitrogen). Fluorescence was imaged on a LSM 700 confocal microscope (Zeiss). Pictures were analyzed and snapshots were taken using Imaris software (version 7.6.5, Bitplane). Ubiquitin and FMRP dots in GFP-positive h-neurons were analyzed using the 3D crop function. The first and last z-planes showing GFP staining were discarded to ensure that ubiquitin and FMRP dots counted were co-localized within GFP-positive h-neurons. We restricted counting of ubiquitin and FMRP dots to dots ≥ 0.5µm, in order to avoid counting of the background staining.

***FMR1* and *FMR1-AS1* promoter sequencing**

FMR1 promoter region (chrX: 147910465-147911958, genome build hg38) was amplified from genomic DNA from primary patient samples (buccal swap or PBMC as indicated in the text) using following primers: FMR1-F1: GGCAGCTATAAGCACGGTGT with FMR1-R2: CCGGAAGTGAAACCGAAAC and FMR1-F6: TCAGCCCTATTGGGTTCTTG with FMR1-R6: AAGGGACATGGATTGAGTCG. FMR1-AS1 promoter region (chrX: 147922071-147922799, genome build hg38) was amplified using following primers: FMR1-AS1-F: CCAGTTTGAGTGCTTTTCAGG with FMR1-AS1-R: ATTTGCAGCCTGCTTTTGAT. PCR amplification was performed using Phusion High-Fidelity PCR master mix (Thermo Scientific) according to the producers' recommendations. Sanger sequencing of the PCR product was performed in both directions with the same primers as for PCR using BigDye Terminator v3.1 kit (Thermo Fisher) and DNA Analyzer 3730xl (Thermo Fisher).

CGG repeat sequencing

CGG repeat in the 5' UTR of *FMR1* and flanking sequences (127bp 5' and 110bp 3' from the repeat) was amplified from genomic DNA of iPSC clones with discrete repeat sizes using AmplideX FMR1 PCR kit (Asuragen) with non FAM modified primers FMR1-F: TCAGGCGCTCAGCTCCGTTTCGGTTTCA with FMR1-R: AAGCGCCATTGGAGCCCCGCACTTCC according to the kit instructions. PCR products were purified with DNA clean & concentrator kit (Zymo Research) and SMRTbell adapters were ligated to them. They were then loaded by diffusion loading onto a Pacific Biosciences RSII sequencer and sequenced using P6-C4 chemistry. Because of the short size of the CGG repeat sequences, we were able to make high quality read-of-insert intramolecular consensuses which were then used for subsequent analysis. The consensus sequences were generated using the cloud-based DNA Nexus computer provider running their cloud app implementation of the PacBio SMRT Analysis v2.3 "read of insert" tool. 500 – 2000 reads containing the full amplicon (CGG repeat and flanking sequences) were obtained from each sample. Alignment of sequences was performed manually using Jalview multiple alignment visualization software (Waterhouse et al., 2009). The alignments were manually inspected for potential alterations in the CGG repeat tract and in the flanking sequences.

Exome sequencing

Exome sequencing was performed for two UFM individuals and their family members indicated in Fig.1 (11 individuals). Primary patient material (buccal swap or PBMC as indicated in the text) was used for genomic DNA

extraction using DNeasy kit (Qiagen). Coding sequences were captured using Agilent SureSelectXT protocol according to manufacturer's instructions. The resulting sequencing libraries were then multiplexed and sequenced on an Illumina HiSeq2500 instrument using TruSeq chemistry with a read length of 2x 76bp. The data is accessible to the FXS research community at the European Genome-Phenome Archive (EGA) (Lappalainen et al., 2015), under accession number EGAS00001001737.

Variant calling followed a standard workflow of Genome Analysis Toolkit (GATK-1.6–11) (McKenna et al., 2010). Sequencing reads were mapped to the human reference genome (GATK b37 bundle version human_g1k_v37_decoy of hg19; GRCh37) using Burrows-Wheeler Aligner (bwa version 0.5.5) (Li and Durbin, 2009) in a paired end mode. Polymerase chain reaction duplicates were removed using picard-tools-1.69 (http://picard.sourceforge.net). Realignment and recalibration were performed using GATK version 1.6-11-g3b2fab9 modules RealignerTargetCreator, IndelRealigner, CountCovariates and TableRecalibration. Reference Indels and SNPs were taken from GATK b37 bundle files Mills_and_1000G_gold_standard.indels.b37.vcf and dbsnp_135.b37.vcf. Variant calling was then performed using GATKlite version 2.3-9-gdcdccbb module UnifiedGenotyper simultaneously for all eleven individuals and restricted to genomic positions covered by the SureSelect kit (bed file provided by the vendor). SNPs and Indels were called in two separate runs. The standard quality parameters stand_call_conf and stand_emit_conf were set to thresholds 30.0 and 10.0 respectively. Low quality variant calls were removed using the GATKlite version 2.3-9-gdcdccbb module VariantFiltration based on quality parameters with separate filtering steps for SNPs and Indels. Filtering rules for exclusion of SNPs were QD < 2, MQ < 40, FS > 60, HaplotypeScore > 13, MQRankSum < -12.5 and ReadPosRankSum < -8. Filtering rules for exclusion of Indels were QD < 2.0, FS > 200 and ReadPosRankSum < -20. Positions with low coverage (less than 66 reads), low quality (QUAL < 30) and long runs of homozygosity (HRun > 5) were excluded. SNPs overlapping with Indels were masked. Clusters of SNPs defined by a clusterSize of 3 with a clusterWindowSize of 10 were also excluded. Annotation of variants was performed using Variant Effect Predictor (VEP) version 2.7 and Ensembl data base version 69 (Cunningham et al., 2015). Variant call vcf files were exported to tabular format using GATKlite version 2.3-9-gdcdccbb module VariantsToTable and further processed wit R version 2.15.2. Final results (variant calls and annotation) were integrated for data mining using Spotfire. (Tibco Software Inc.).

90084 variants (SNPs and indels) were identified in one or both UFMs. A list of 2607 genes broadly implicated in epigenetic processes was assembled using internal databases, publications and online resources ((Bartke et al., 2010; Fodor et al., 2010; Gao et al., 2012; Hamperl and Cimprich, 2014; Hu et al., 2010; Spruijt et al., 2013), http://sciencepark.mdanderson.org/labs/wood/DNA_Repair_Genes). Transcription factors predicted to bind *FMR1* promoter based on search with Genomatix MatIspector software were included in the list (www.genomatix.com). Full list of candidate genes is provided in Table S2. Variants were filtered for ones affecting the coding sequence of these genes (frameshift, initiator codon change, STOP codon change, missense, in-frame sequence change), resulting in 1623 variants. Variants present in at least one FXS individual were excluded (Variants homozygous in UFM and heterozygous in FXS were kept), resulting in 295 variants present in at least one UFM. Further, 68 variants affecting the same gene (same or different variant) in both UFM individuals were selected and are provided in Table S3. These variants were further evaluated for the impact on the protein function using manual sequence inspection, literature, and SIFT and Polyphen scores for missense mutations.

Supplemental References

Bartke, T., Vermeulen, M., Xhemalce, B., Robson, S.C., Mann, M., and Kouzarides, T. (2010). Nucleosome-interacting proteins regulated by DNA and histone methylation. Cell *143*, 470-484.

Chambers, S.M., Fasano, C.A., Papapetrou, E.P., Tomishima, M., Sadelain, M., and Studer, L. (2009). Highly efficient neural conversion of human ES and iPS cells by dual inhibition of SMAD signaling. Nat Biotechnol *27*, 275-280.

Cunningham, F., Amode, M.R., Barrell, D., Beal, K., Billis, K., Brent, S., Carvalho-Silva, D., Clapham, P., Coates, G., Fitzgerald, S., *et al.* (2015). Ensembl 2015. Nucleic Acids Res *43*, D662-669.

Filipovic-Sadic, S., Sah, S., Chen, L., Krosting, J., Sekinger, E., Zhang, W., Hagerman, P.J., Stenzel, T.T., Hadd, A.G., Latham, G.J., *et al.* (2010). A novel FMR1 PCR method for the routine detection of low abundance expanded alleles and full mutations in fragile X syndrome. Clin Chem *56*, 399-408.

Fodor, B.D., Shukeir, N., Reuter, G., and Jenuwein, T. (2010). Mammalian Su(var) genes in chromatin control. Annu Rev Cell Dev Biol *26*, 471-501.

Gao, Z., Zhang, J., Bonasio, R., Strino, F., Sawai, A., Parisi, F., Kluger, Y., and Reinberg, D. (2012). PCGF homologs, CBX proteins, and RYBP define functionally distinct PRC1 family complexes. Mol Cell *45*, 344-356.

Hamperl, S., and Cimprich, K.A. (2014). The contribution of co-transcriptional RNA:DNA hybrid structures to DNA damage and genome instability. DNA Repair (Amst) *19*, 84-94.

Hu, X.V., Rodrigues, T.M., Tao, H., Baker, R.K., Miraglia, L., Orth, A.P., Lyons, G.E., Schultz, P.G., and Wu, X. (2010). Identification of RING finger protein 4 (RNF4) as a modulator of DNA demethylation through a functional genomics screen. Proc Natl Acad Sci U S A *107*, 15087-15092.

Lanni, S., Goracci, M., Borrelli, L., Mancano, G., Chiurazzi, P., Moscato, U., Ferre, F., Helmer-Citterich, M., Tabolacci, E., and Neri, G. (2013). Role of CTCF protein in regulating FMR1 locus transcription. PLoS Genet *9*, e1003601.

Lappalainen, I., Almeida-King, J., Kumanduri, V., Senf, A., Spalding, J.D., Ur-Rehman, S., Saunders, G., Kandasamy, J., Caccamo, M., Leinonen, R., *et al.* (2015). The European Genome-phenome Archive of human data consented for biomedical research. Nat Genet *47*, 692-695.

Li, H., and Durbin, R. (2009). Fast and accurate short read alignment with Burrows-Wheeler transform. Bioinformatics *25*, 1754-1760.

McKenna, A., Hanna, M., Banks, E., Sivachenko, A., Cibulskis, K., Kernytsky, A., Garimella, K., Altshuler, D., Gabriel, S., Daly, M., *et al.* (2010). The Genome Analysis Toolkit: a MapReduce framework for analyzing next-generation DNA sequencing data. Genome Res *20*, 1297-1303.

Naumann, A., Hochstein, N., Weber, S., Fanning, E., and Doerfler, W. (2009). A distinct DNA-methylation boundary in the 5'- upstream sequence of the FMR1 promoter binds nuclear proteins and is lost in fragile X syndrome. Am J Hum Genet *85*, 606-616.

Smurnyy, Y., Cai, M., Wu, H., McWhinnie, E., Tallarico, J.A., Yang, Y., and Feng, Y. (2014). DNA sequencing and CRISPR-Cas9 gene editing for target validation in mammalian cells. Nat Chem Biol *10*, 623-625.

Spruijt, C.G., Gnerlich, F., Smits, A.H., Pfaffeneder, T., Jansen, P.W., Bauer, C., Munzel, M., Wagner, M., Muller, M., Khan, F., *et al.* (2013). Dynamic readers for 5-(hydroxy)methylcytosine and its oxidized derivatives. Cell *152*, 1146-1159.

Tsoukas, C.D., Landgraf, B., Bentin, J., Valentine, M., Lotz, M., Vaughan, J.H., and Carson, D.A. (1985). Activation of resting T lymphocytes by anti-CD3 (T3) antibodies in the absence of monocytes. J Immunol *135*, 1719-1723.

Waterhouse, A.M., Procter, J.B., Martin, D.M., Clamp, M., and Barton, G.J. (2009). Jalview Version 2--a multiple sequence alignment editor and analysis workbench. Bioinformatics *25*, 1189-1191.